1966

A study of noncoherent rotation switching for thin magnetic films

John Honett Hoper
Iowa State University

66–10,425

HOPER, John Honett, 1940–

A STUDY OF NONCOHERENT ROTATION SWITCHING FOR THIN MAGNETIC FILMS.

Iowa State University of Science and Technology
Ph.D., 1966
Engineering, electrical
Physics, solid state

University Microfilms, Inc., Ann Arbor, Michigan

A STUDY OF NONCOHERENT ROTATION SWITCHING FOR THIN MAGNETIC FILMS

by

John Honett Hoper

A Dissertation Submitted to the
Graduate Faculty in Partial Fulfillment of
The Requirements for the Degree of
DOCTOR OF PHILOSOPHY

Major Subject: Electrical Engineering

Approved:

Signature was redacted for privacy.

In Charge of Major Work

Signature was redacted for privacy.

Head of Major Department

Signature was redacted for privacy.

Dean of Graduate College

Iowa State University
Of Science and Technology
Ames, Iowa

1966

TABLE OF CONTENTS

		Page
I.	INTRODUCTION	1
II.	EXPERIMENTAL APPARATUS	6
	A. Introduction	6
	B. Pulse Field System	6
	C. Steady and Reset Fields	13
	D. Sensing System	14
	E. Impulse Response	20
	F. Logic System	23
III.	EXPERIMENTAL RESULTS	26
	A. Introduction	26
	B. Longitudinal and Transverse Voltage Wave Forms (LVW,TVW)	27
	C. Switching Times for Fast Rotation	30
	D. Flux Switched by Fast Rotation	36
	E. Trajectories of the Magnetization	48
	F. Reversability	54
IV.	THEORETICAL RESULTS	65
	A. Introduction	65
	B. Filter	65
	C. Rotation Model	69
	D. Spin-Wave Model	70
	E. Strip Domain Model	77
V.	CONCLUSIONS	83
VI.	LITERATURE CITED	85
VII.	ACKNOWLEDGMENTS	87

		Page
VIII.	APPENDIX A	88
	General Equations of Motion	88
IX.	APPENDIX B	90
	Rotation Model	90
X.	APPENDIX C	94
	Spin-Wave Model	94
XI.	APPENDIX D	96
	Strip Domain Model	96
	Large angle calculation	96
	Small angle calculation	98

I. INTRODUCTION

The first investigation of the preparation and magnetic properties of thin ($\sim$1000 Å), 80-20 permalloy films was by Blois in 1955. (1) He found that if a steady magnetic field was applied in the plane of the film during vacuum-evaporation, a uniaxial anisotropy was induced in the direction of the field. The film could then exist as a single domain, and with no external applied fields, the magnetization could lie parallel or anti-parallel to this induced "easy axis". By applying a small magnetic field ($\sim$3 oe), the direction of the magnetization could be reversed. With the possibility of using magnetic films as a bistable memory element, much research was done to characterize the processes of magnetization reversal. A number of excellent articles reviewing the literature have been written. (1,2,3,4,5) Fig. 1, a plot of inverse switching times for reversal versus applied field, illustrates these experimental findings. Note the three general regions.

In region 1 reversal is by wall motion where walls are nucleated at the edges and imperfections, creating domains with the magnetization anti-parallel to its initial direction. These new domains grow by the movement of the walls, completing the switching. (5, p 170)

In region 3 the magnetization does not split into domains, but rotates coherently. According to a simple energy picture (5, p 159) as soon as the applied field energy exceeds the anisotropy energy, rotation occurs. As can be seen, the switching time for this process is the fastest. There are several discrepancies in the pure rotation model concept. One is an apparent damping constant for large angle rotation two to three times the value obtained from free oscillations of the magnetization and

Fig. 1. Switching characteristics of a thin magnetic film showing these three regions - 1) wall motion - 2) noncoherent rotation - 3) coherent rotation (after Olson and Pohm (4))

Fig. 2. Electron micrograph (courtesy of M. S. Cohen, M.I.T., Lincoln Labs) of a thin magnetic film showing domain walls (heavy black and white lines) and magnetization ripple (fine structure)

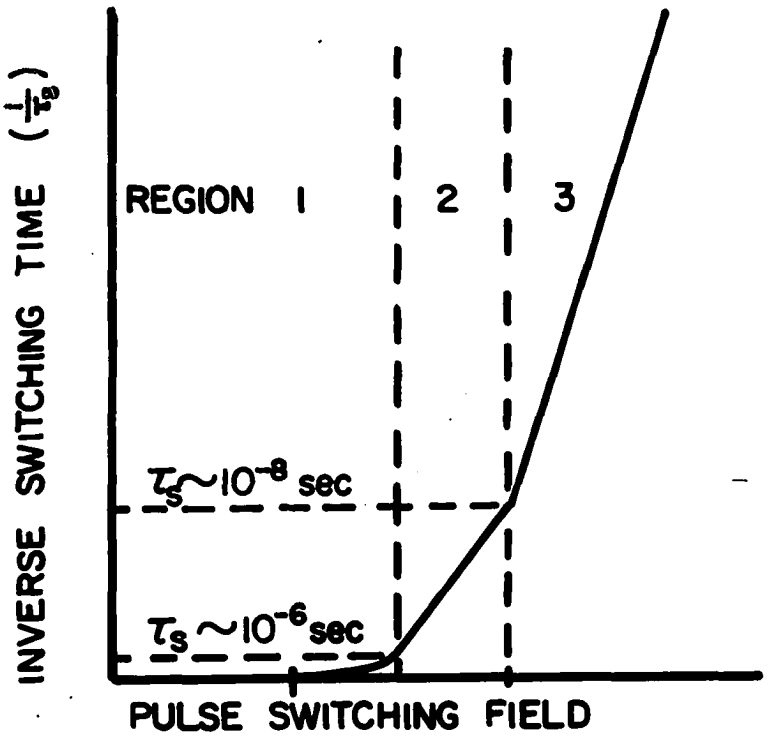
INVERSE SWITCHING TIME ($\frac{1}{\tau_s}$)
REGION 1
2
3
$\tau_s \sim 10^{-8}$ sec
$\tau_s \sim 10^{-6}$ sec
PULSE SWITCHING FIELD

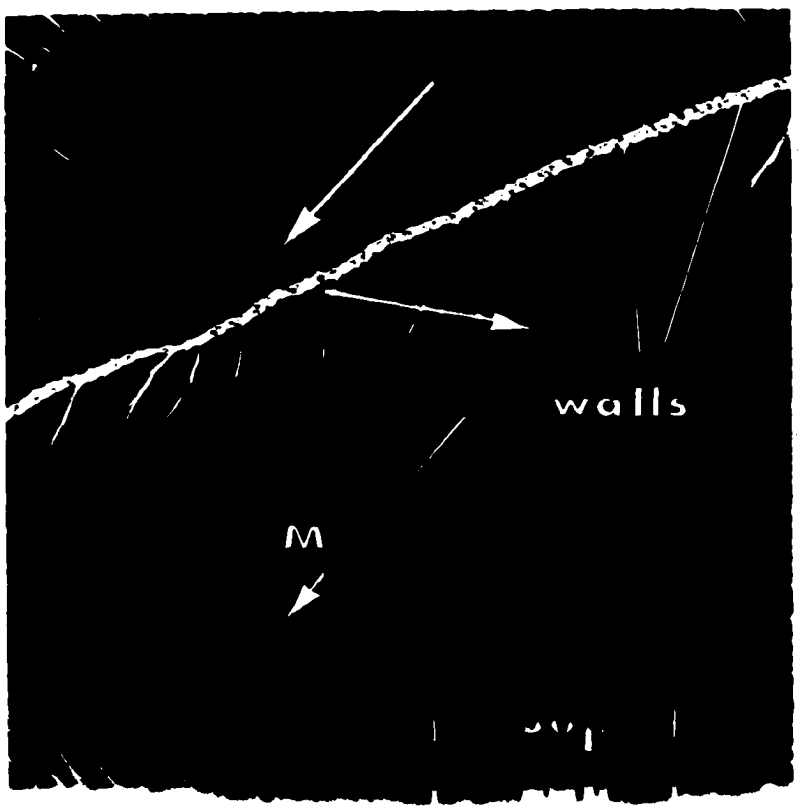
walls
M

small angle resonance. (6,7,8) The other is that rotation does not occur unless the applied fields are considerably larger ($\sim$1.5) than the calculated critical fields. Smith and Harte (8) attributed the latter discrepancy to the dispersion of the amplitude and direction of the uniaxial anisotropy. They stated that coherent rotation is controlled by the regions of high anisotropy. However, interactions between regions were neglected. When a magnetic film is observed through a defocused electron microscope, a fine structure of the magnetization called magnetization ripple is seen. (9) Fig. 2 is an example of an electron micrograph (courtesy of M. S. Cohen, M.I.T. Lincoln Labs). The solid black and white lines denote domain walls, while the variations perpendicular to the net magnetization are called ripple. The effects of the nonuniformity of the magnetization were taken into account by Harte (6) in an attempt to answer the two discrepancies with the pure rotation model. However, his basic premise that the initial ripple does not relax before the net magnetization has switched does not agree with the experimental results. This model will be discussed in much greater detail in Chapter 4.

In region 2 the magnetization first starts to switch by fast rotation, then by a much slower mechanism. Hence, it is called noncoherent rotation. The resulting voltage wave form of the switching signal is a fast spike ($\sim$5 nsec.) followed by a long tail ($\sim$100 nsec.) shown in Fig. 39. There have been many proposed models for the anomalous behavior in region 2. Harte (10) attributed it to the dispersion of the anisotropy, but again magnetostatic interactions were neglected. A number of models explaining the slow mechanism have been based on static observations. D. O. Smith (8) has observed a process of switching by labyrinth propagation which is

essentially the motion of the tip of a new domain. However, Methfessel et al. (11) have observed a partial rotation process where the magnetization breaks into domains perpendicular to the net magnetization as the applied fields approach the Stoner-Wohlfarth critical fields. (12) Thomas (13) has proposed a strip domain model describing this static process. Stein (14), by interrupting the film switching during the nonhomogenous rotation and then observing the resulting domain configuration with a Kerr apparatus, concludes that a strip domain picture is the correct one. Harte (6) shows that spin-waves can apply a large enough torque on the net magnetization to lock it from further rotation, and then he conjectures that rotation slowly proceeds as the spin-waves relax.

Much of the data concerning regions 2 and 3 was obtained prior to 1960. The equipment that was used had rise times around 3 nsec., and the information received was considerably distorted. Two good examples of this distortion are 1) no oscillations of the magnetization were observed during switching and 2) switching times were <u>much</u> slower than the rotation model predicted. (See Fig. 15 and discussion on page 69.) The apparatus of Dietrich and Proebster (15) had the fast rise time needed, but lacked the sensitivity desired to observe small signals near the switching thresholds.

The purpose of the research for this thesis, therefore, was 1) to construct a high sensitivity, fast rise time apparatus, 2) to make measurements for applied fields near the critical thresholds, 3) and to compare the measurements with the results predicted by the strip domain (13), spin-wave (6), and pure rotation (16) models.

II. EXPERIMENTAL APPARATUS

A. Introduction

The basic experimental problem was to build an apparatus to apply a fast rise time field (∿.25 nsec.) in the plane of the thin film and then detect how the film behaves. This was done as shown schematically in Fig. 3. The pulse field was applied only in the longitudinal direction, but steady bias fields could be applied in both the longitudinal and transverse directions.

Any changes of either the angle or the magnitude of the magnetization would cause a change of flux in the two mutually perpendicular pick-up loops (sense coils). The voltages out of the longitudinal and transverse coils were

$$V_T = K_T \frac{dM_T}{dt} \tag{1}$$

$$V_L = K_L \frac{dM_L}{dt} \tag{2}$$

where K_T and K_L depend on sense coil and thin film geometry.

B. Pulse Field System

The fast rise time (∿.25 nsec.) magnetic field was generated by discharging a previously charged 50Ω coaxial cable through a mercury switch relay into a shorted 50Ω transmission line called the field pulser, Fig. 4. This launched a TEM electromagnetic field which traveled down the transmission line and was reflected at the short. Here the voltage was zero and the current was doubled. By placing the film near the short, the effective field was doubled and the capacitive coupling noise to the

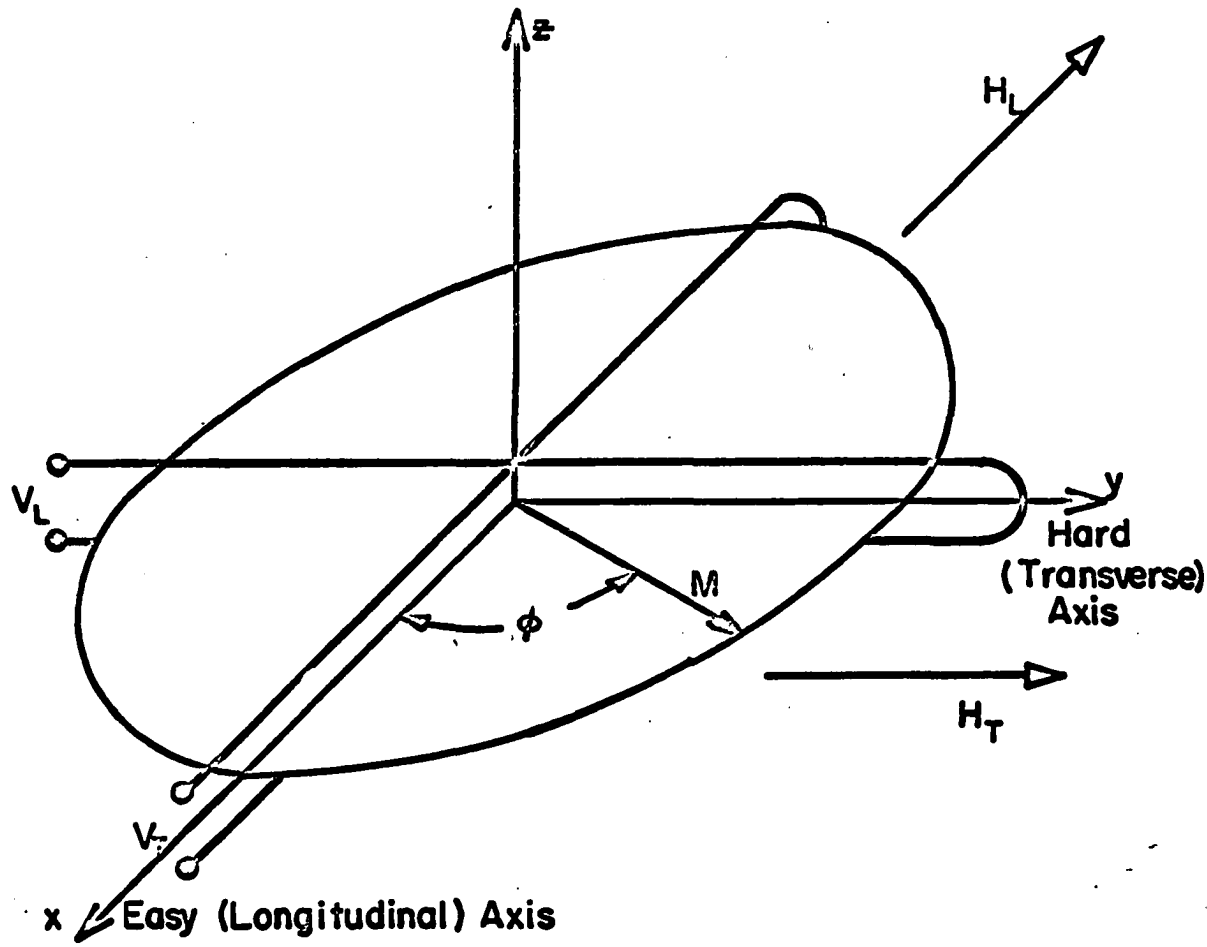

Fig. 3. Schematic drawing of thin film coordinate system showing applied fields and placement of sense coils

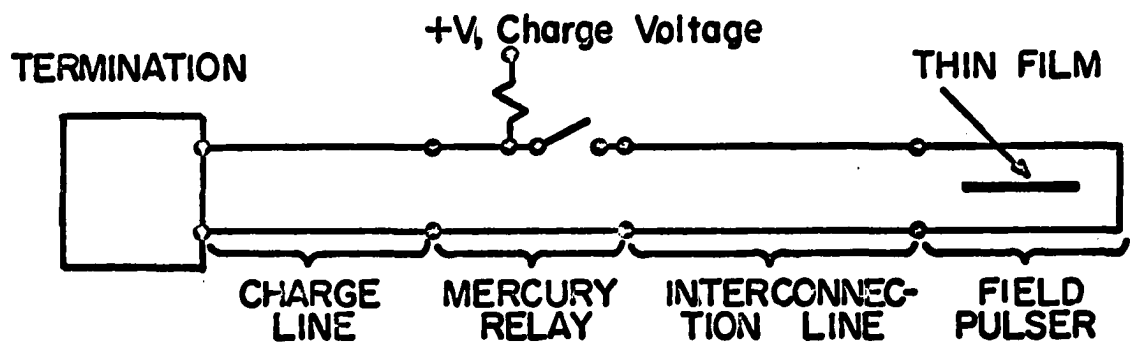

Fig. 4. Pulse field system

pick-up coils was reduced by orders of magnitude. The field pulse could be varied both in magnitude, by changing the charge voltage V, and in duration, T, by using different length charge lines where

$$T = 2T_c \tag{3}$$

and T_c = time for an electromagnetic wave to travel the length of the charge line.

When the mercury switch was closed, the resulting wave was a superposition of two waves propagating in opposite directions in the charge line. The wave traveling towards the termination was reflected there with a reflection coefficient of one. (See the detailed description of the terminations.) It then traveled out towards the field pulser. The overall result was a pulse with a voltage amplitude of V/2 and duration $2T_c$.

The field pulser was constructed from a 5/8 inch overall diameter copper tube pressed into the configuration shown in Fig. 5. The center conductor width and placement were chosen to make the calculated fields uniform to within 3% for 3mm diameter magnetic film samples. The characteristic impedance of the pulser was adjusted to 50 $\pm$ 2Ω with the use of a Hewlett-Packard time domain reflectometer. A 1/4 inch hole drilled in the outer conductor over the sense coils was used to observe bitter patterns. During the switching measurements, a copper plug was placed in the hole.

The calibration of the fields in the pulser was obtained by using the peak value of a longitudinal voltage signal from a thin film as a reference. After recording this peak value, a steady field ($H_{dc} << H_{pulse}, H_K$) was applied parallel to the pulse field. In order to keep a constant voltage

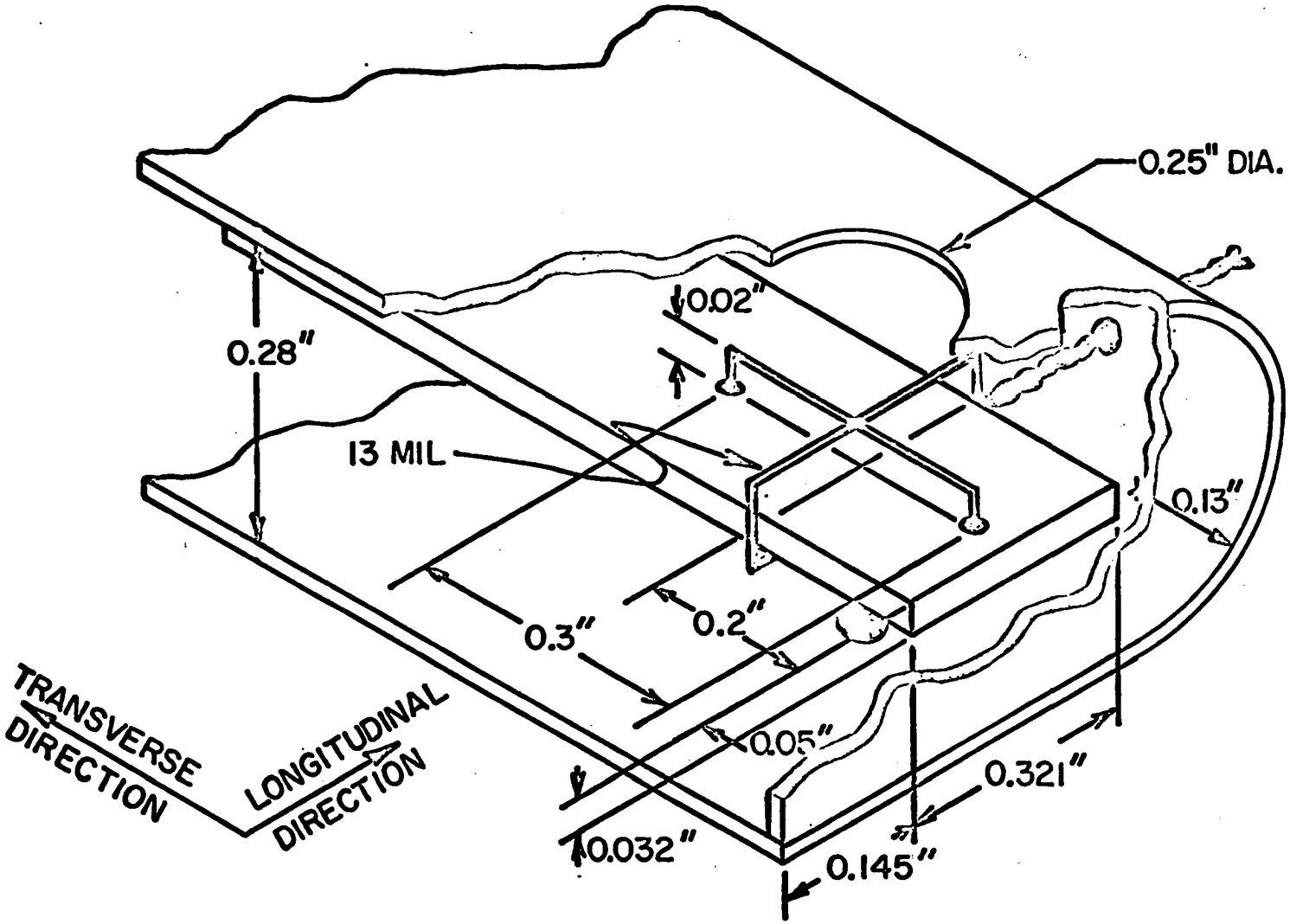

Fig. 5. Field pulser and sense coil arrangement

amplitude, the pulse field needed to be reduced by the magnitude of the D.C. field (decrease the charge voltage). Since the change in the charge voltage for a given change in field was known, the pulser was then calibrated. The value obtained agreed within 10% of the calculated value. Using a 0 to 500 volt charge voltage, a 0 to 5.5 oersted pulse was obtained.

Terminations were used not only to eliminate multiple reflections, but to obtain various wave forms as shown in Fig. 6.

Briefly, the 6a termination was to prevent multiple reflections. Initially, the diode was back biased and looked like an open circuit. When the voltage wave reflected from the field pulser and arrived at the termination, the diode then conducted. With the series resistor, the impedance of the termination was then 50Ω, thus dissipating the wave.

The field doubler, Fig. 6b, worked in the following manner. The capacitor was initially charged up to V volts. When the relay was closed, the capacitor looked like a zero internal impedance voltage source for time < $Z_o C$ where Z_o = 50Ω and C = .01 μfarad. Here

T_c = propagation time through charge cable

T_i = propagation time through interconnection cable.

The attenuation from the coaxial cables kept the fields from building up to large values.

The termination, Fig. 6c, was very similar to Fig. 6b and was used for generating field pulses of equal amplitude. The capacitor was charged up to K•V where $K = R_2/(R_1+R_2)$, while the coaxial cable was at V volts. Hence, the diode was initially back biased and isolated the capacitor. At time T_c after the switch was closed, the amplitude of the voltage wave

Fig. 6. Terminations for the charge lines and the resulting pulse fields

a. Termination to prevent multiple reflections

b. Termination to double pulse field

c. Termination to generate equal amplitude pulses

T_i - propagation time through interconnection cable

T_c - propagation time through charge cable

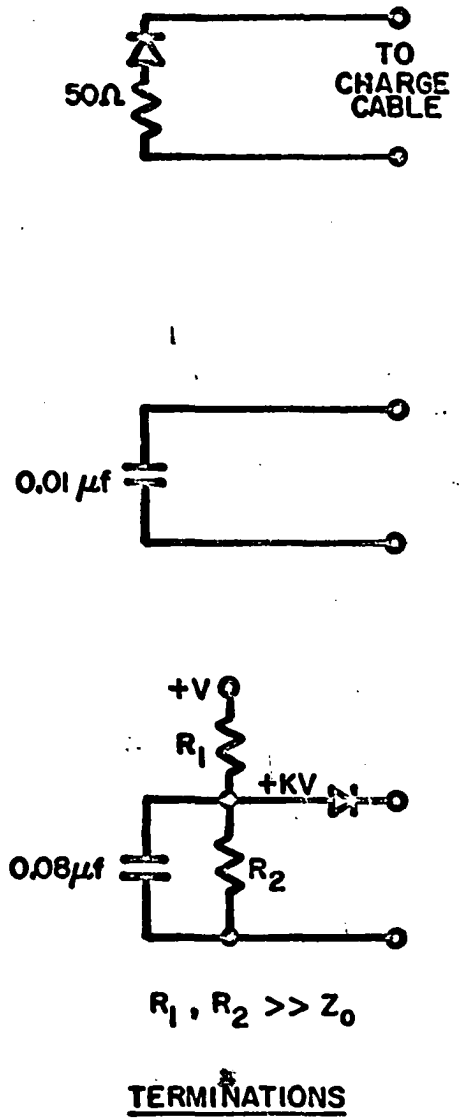

TERMINATIONS

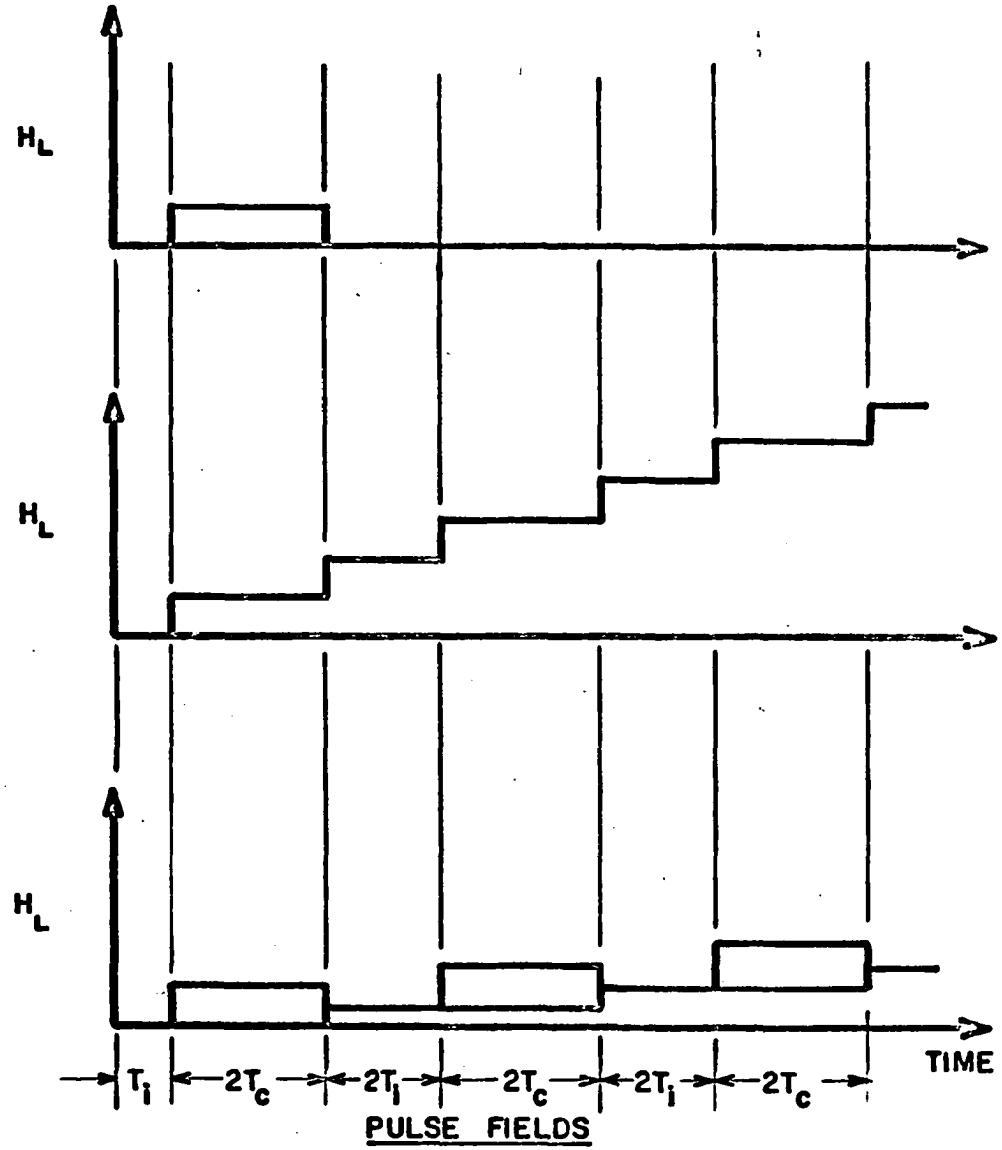

PULSE FIELDS

was zero at the termination, so the diode then conducted. Since the voltage waves from the field pulser were always negatively reflected, the diode then conducted "forever" and could be ignored in the following analysis. Therefore, after time T_c, the termination looked like a voltage source K•V with zero internal impedance. The reason for having this voltage source was to compensate for the attenuation in the cables. Consequently, consecutive pulses were of equal magnitude. By this method the time between pulses, $2T_i$, could be varied from 10 to 200 nsec. by changing the length of the interconnection cable.

C. Steady and Reset Fields

After applying the pulse field, the film was then switched back to its previous state by using a ~10 oersted field parallel to the longitudinal direction with a Helmholtz coil external to the pulser. To make sure this field penetrated through the outer conductor of the pulser and then died away before the measurements were made, the eddy current time constant for the pulser was considered. When calculated and measured, it was found to be < .2 msec. With a repetition rate in the experiment of 3 msec. and the use of a .5 msec. reset pulse, these eddy currents caused no problems.

Steady fields continuously variable from 0 to 5 oersted could be independently applied parallel and/or antiparallel to the transverse and longitudinal directions, again using two orthogonal Helmholtz coils. These coils were wound on brass rings to decouple them from extraneous noise. The time constant for the eddy currents in the rings was measured to be 75 μsec. Therefore, the transverse field could be turned on and off

at the required 3 msec. rate. (See Fig. 13)

The earth's magnetic field was detected with a Hewlett-Packard magnetometer and cancelled to within a few millioersteds by a permanent magnet.

D. Sensing System

In order to measure the small flux changes produced by the magnetic film, the pick-up coils had to be designed and constructed properly. Otherwise, noise would have completely overshadowed the signal. For example, the typical voltage amplitude in the pulse system was 200 volts, whereas the detected signals were around 10 mV. There were four basic types of noise that needed to be minimized.

1. Extraneous--These were due to radio stations, ham operators, etc. Since the field pulser only had one open side (Fig. 5), its outer conductor shielded the sense coils, so this type of noise was negligible. Also, twisted pair and coaxial cable were used exclusively throughout the system.

2. Inductive noise from the applied field pulse--If the coil perpendicular to the longitudinal direction was made as shown in Fig. 3, the coil would not only sense the film, but the applied field flux changes as well. Since a magnetic field is circumferential about a current, the sense coil was placed symmetrically about the center conductor. The <u>total</u> flux through the coil from the applied field would then be zero. Hence, the inductive noise was eliminated (Fig. 7).

3. Capacitive noise--Even with the sense coils close to the point where the center conductor was shorted to the outside conductor, the amplitude of the applied voltage wave at the coils was not exactly zero. With the sense coils floating electrically from the center conductor,

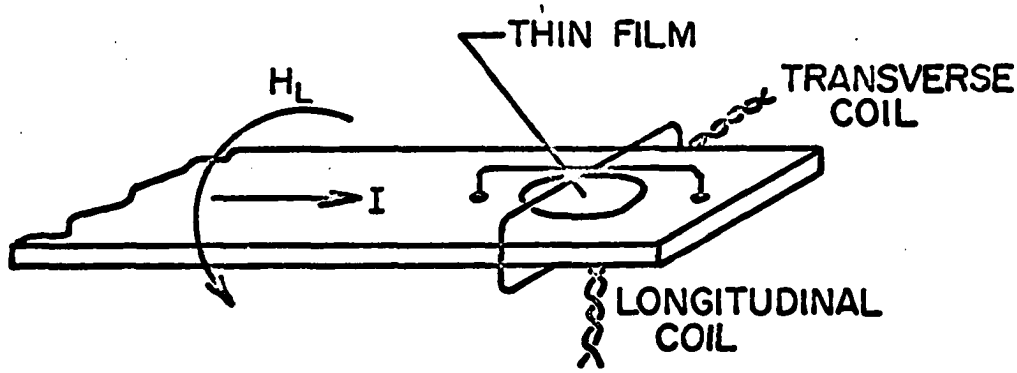

Fig. 7a. Pictorial of the sense coils and center conductor

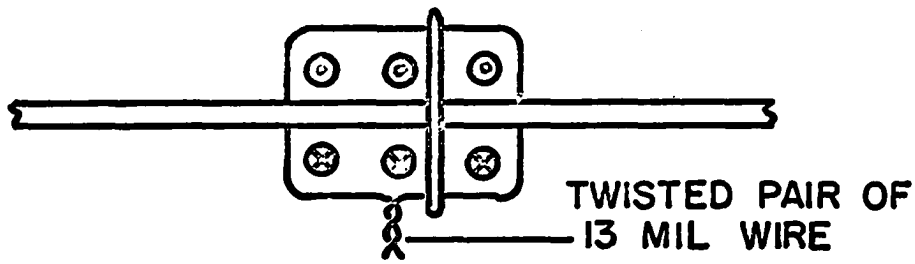

Fig. 7b. Pulse fields in the longitudinal coil showing inductive noise cancelation

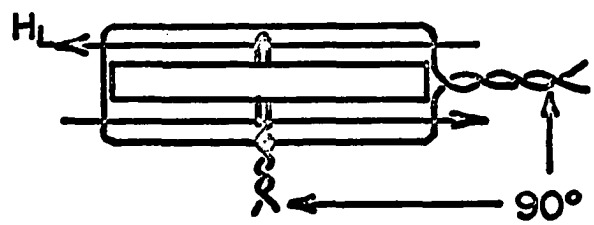

Fig. 7c. Coil configuration looking in the transverse direction

there was a resulting capacity of approximately a pfarad between the two. This gave ∿3 volts noise compared to ∿.1 volt signal. The capacity could have been reduced by increasing the size of the coils, but this would have seriously reduced the rise time of the system.

What was done for the longitudinal sense coil is shown in Fig. 8, where V_N was the voltage of the applied voltage wave at the sense coil, C was the capacitance between the sense coil and the center conductor, and Z_o was the characteristic impedance between the twisted pair and the outer conductor. Analyzing it by transmission line techniques, there were two waves picked up by the sense coil--the sense wave propagating between the two wires of the twisted pair and the capacitively induced noise propagating between the twisted pair as a whole and the ground plane (pulser's outer conductor). The object was to terminate the noise wave without disturbing the signal wave. This was done by using a balun (17) which was made by treating the twisted pair as a single conductor and winding it around a ferrite toroid. This high permeability material did not appreciably effect the signal wave because the fields were highly localized between the two conductors. However, the noise wave saw a large inductance (1 μhenry). By placing resistors equal to the characteristic impedance but much less than the toroid reactance in front of the balun, the noise wave was properly terminated. A piece of carbon was placed on the outer conductor so that if there were multiple reflections, they would be highly attenuated. Because of the transverse coil's geometry, the noise was low enough so that only the toroid and carbon attenuater were needed.

4. Noise from impedance mismatch--Any discontinuities in the characteristic impedance of the transmission line from the sense coil to the

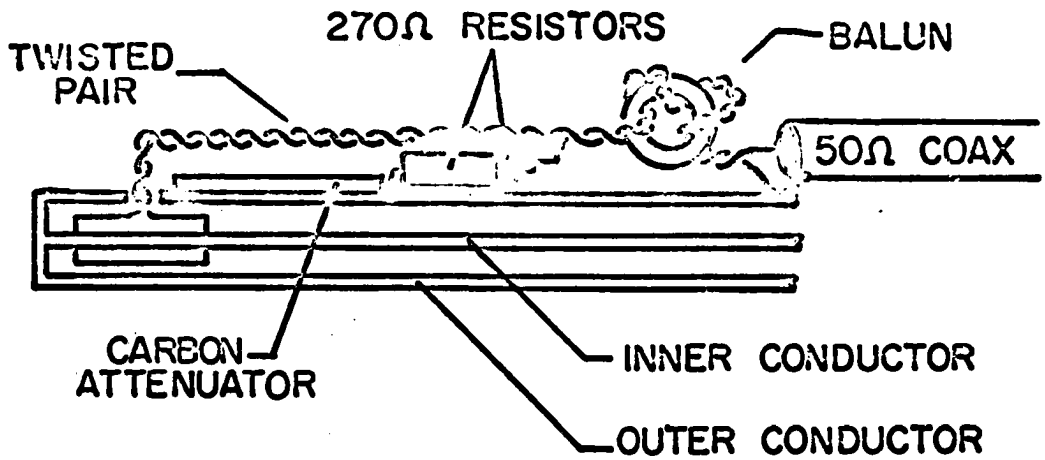

PHYSICAL SYSTEM

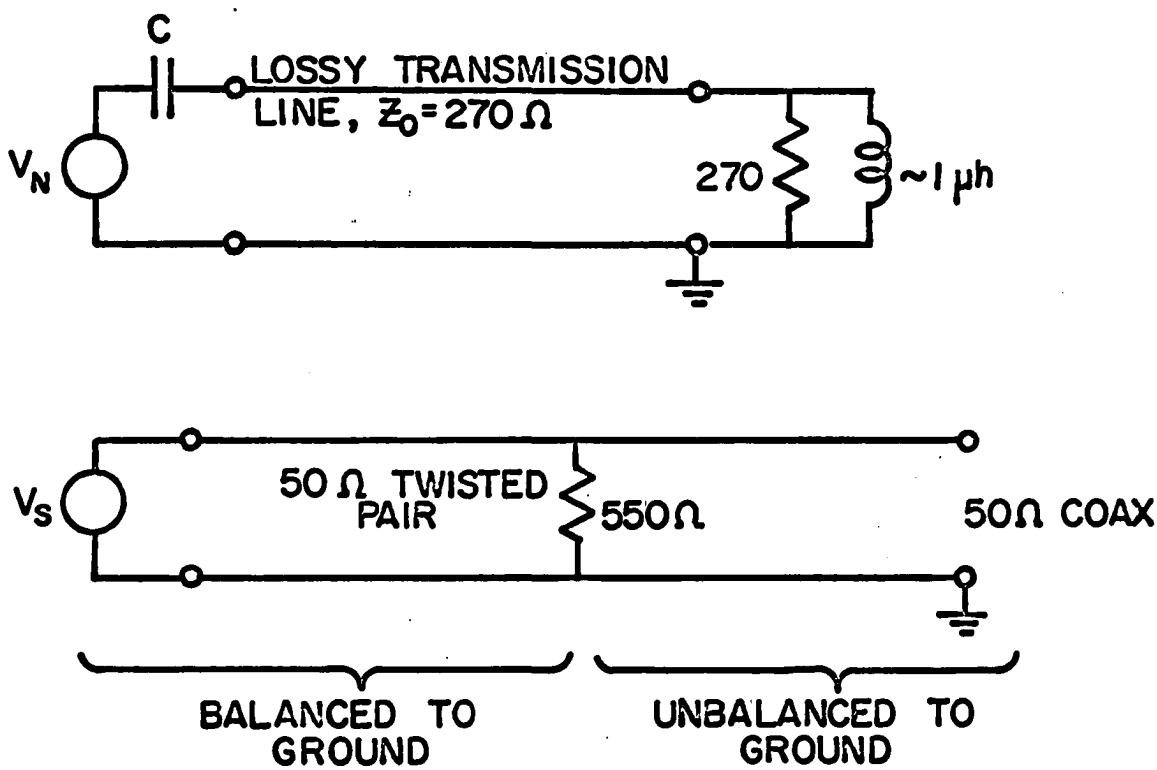

ELECTRICAL EQUIVALENT

Fig. 8. Cancelation scheme for capacitive noise
V_N - noise voltage, V_S - signal voltage

sampling oscilloscope would cause part of the signal to be reflected back to the sense coil. Here it would be inverted and returned, causing ringing and distortion of the signal. To eliminate mismatch, the time domain reflectometer was used to check the impedance of the twisted pair and all the connections.

To further increase the signal to noise ratio, an electronic substracter was used. (18) The basic idea was to alternately supply signals 1 and 2 to the sampling oscilloscope.

signal 1--remaining uncancelled noise plus signals produced by the magnetic film

signal 2--remaining uncancelled noise

The resulting wave form that appeared on the oscilloscope consisted of alternating segments of signal plus noise and noise simulated in Fig. 9A. By then doing a segment by segment subtraction, the noise was cancelled and only the signal remained. This was done electronically by a clamping circuit which is shown schematically in Fig. 9B. When the switch was closed during the noise segment, the capacitor charged to V_N. By opening the switch during the signal plus noise portion, $(V_S + V_N) - V_N$ or V_S appeared at V_o. This wave form is shown in Fig. 9C. By having another clamping circuit with the switch open during the noise and closed during the signal plus noise, the resulting wave form was $-V_S$ (or, in other words, inverted). If the voltages from those two clamping circuits were put into a difference amplifier, (two operational amplifiers of an analog computer were used) a single, continuous wave form was obtained. Any extraneous noise (60 H_Z, jitter, etc.) would appear as fuzz on the wave form and could be removed by using a low-pass filter without degregating the desired

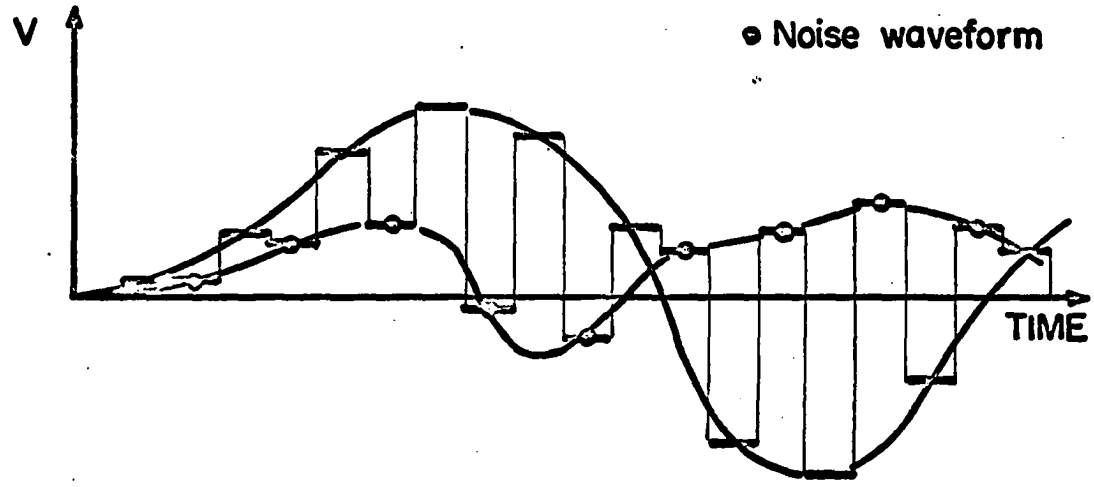

(A) Sampled wave form input

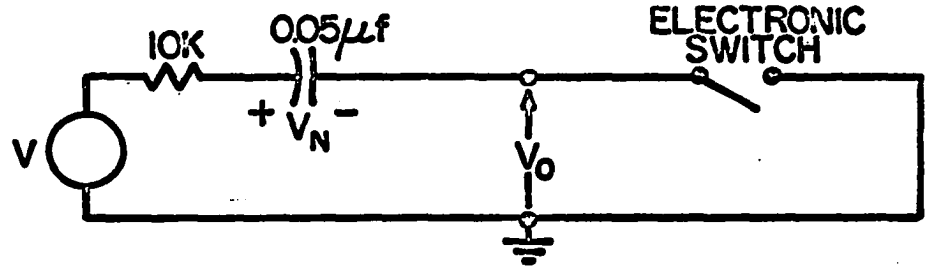

(B) Schematic diagram of the clamping circuit

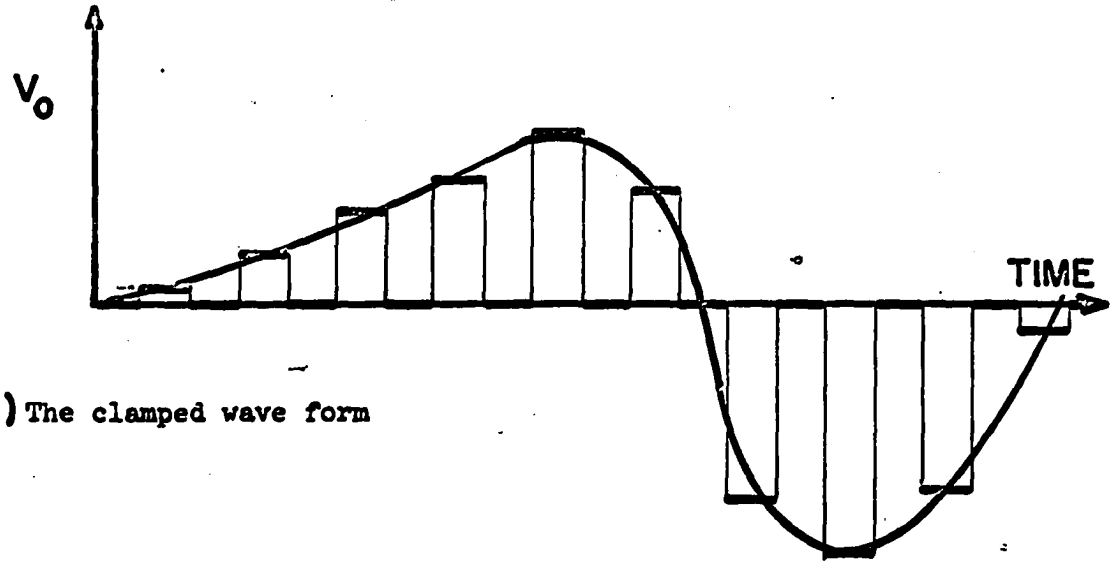

(C) The clamped wave form

Fig. 9. Electronic subtractor

information. Essentially, this filter just averaged out uncorrelated fluctuations. Two examples of what this noise reducer could do are shown in Figs. 10 and 11. Fig. 11 is the first few nsec. of Fig. 10, showing the "notch" in detail.

What remains to be explained is how the two wave forms were obtained.

The signal plus noise wave form was the resulting signal when both the "steady" transverse and the longitudinal pulse fields were applied. Before the switched film was reset to its initial state, the pulse field was applied again, but now with zero transverse field. Because the magnetization was aligned with the field, no film signal was observed--only the noise. The magnetization was then reset to its initial state and the "steady" transverse field reapplied, etc.

E. Impulse Response

In Chapter 4 the voltage wave forms of various proposed models for thin film switching will be calculated. However, to compare these wave forms with experimental ones, it would be helpful to know how the measuring apparatus or sensing system (pick-up coils, coaxial cables to oscilloscope, and the sampling oscilloscope itself) would distort the theoretical voltages. In essence this was taking into account the "noise" due to the sense system's finite rise time and reflections. The problem was solved once the impulse response of the sense system was known. Then the convolution integral would be used to filter the ideal voltages. (19, p 115)

Experimentally, the major difficulty was to obtain a signal that looked like an impulse to a .6 nsec. rise time system. This was done with the help of the time domain reflectometer. The step output with a 50 psec.

Fig. 10. Example using electronic subtracter - film 1, $H_T = .3\ H_K$, $H_L = .5\ H_K$, 1 nsec/cm, 20 mv/cm

Fig. 11. First portion of Fig. 10 - .2 nsec./cm, 10 mv/cm

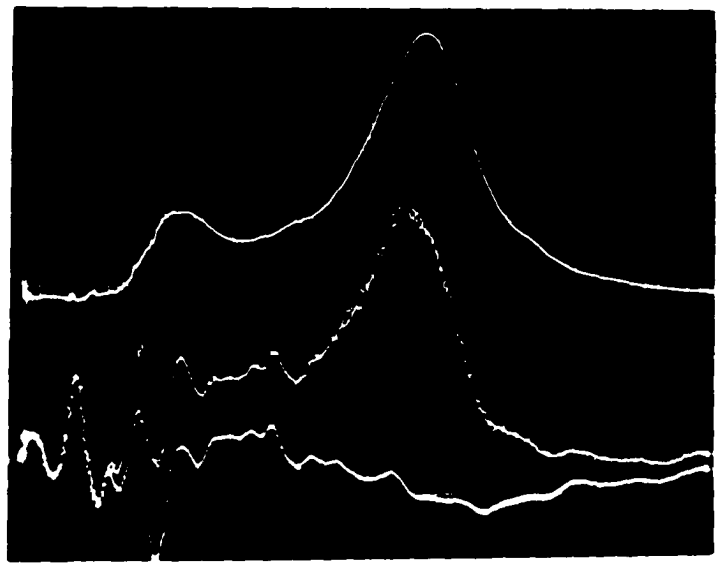

rise time from this instrument was fed into a 50Ω coaxial cable terminated with a small loop antenna. This antenna with an area less than one square mm was placed near the sense coils. The sense coils detected the derivative of the resulting step, transmitted field which was an impulse. The sensed signal was fed into the Tektronic sampling scope. The resulting trace was the overall sensing system impulse response shown in Fig. 40.

F. Logic System

The coordination for the various circuits such as the electronic subtractor, reset fields, etc. was done with a binary counter. This counter was triggered every time a field pulse was applied to the thin film by the free running pulse generator. To avoid disturbing any measurements, all logic changes, with the exception of the delay circuit, were made 2 μsec. after the field pulse. A block diagram is shown in Fig. 12, with the time sequence of the various fields, etc. in Fig. 13.

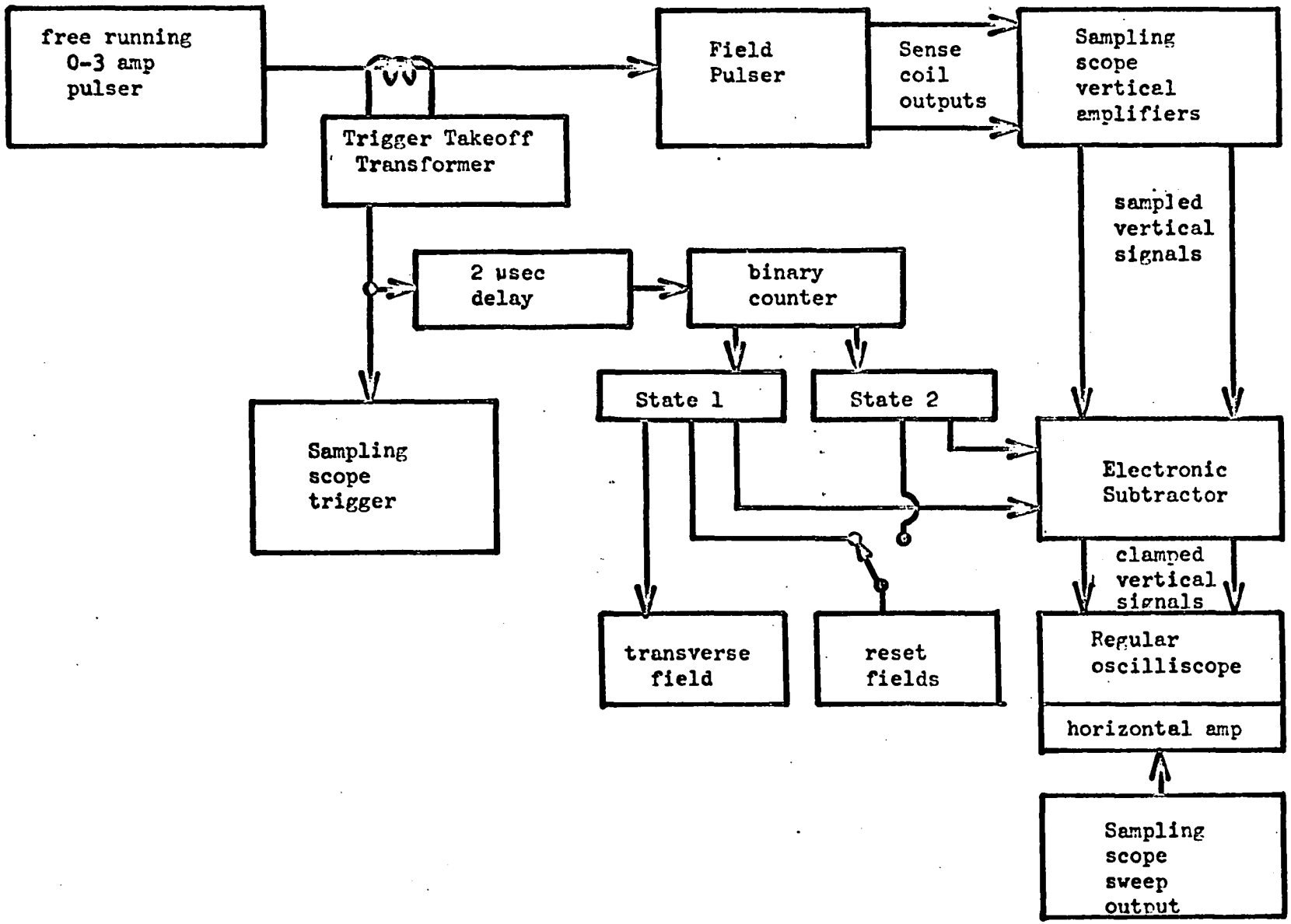

Fig. 12. Logic diagram for the experimental apparatus

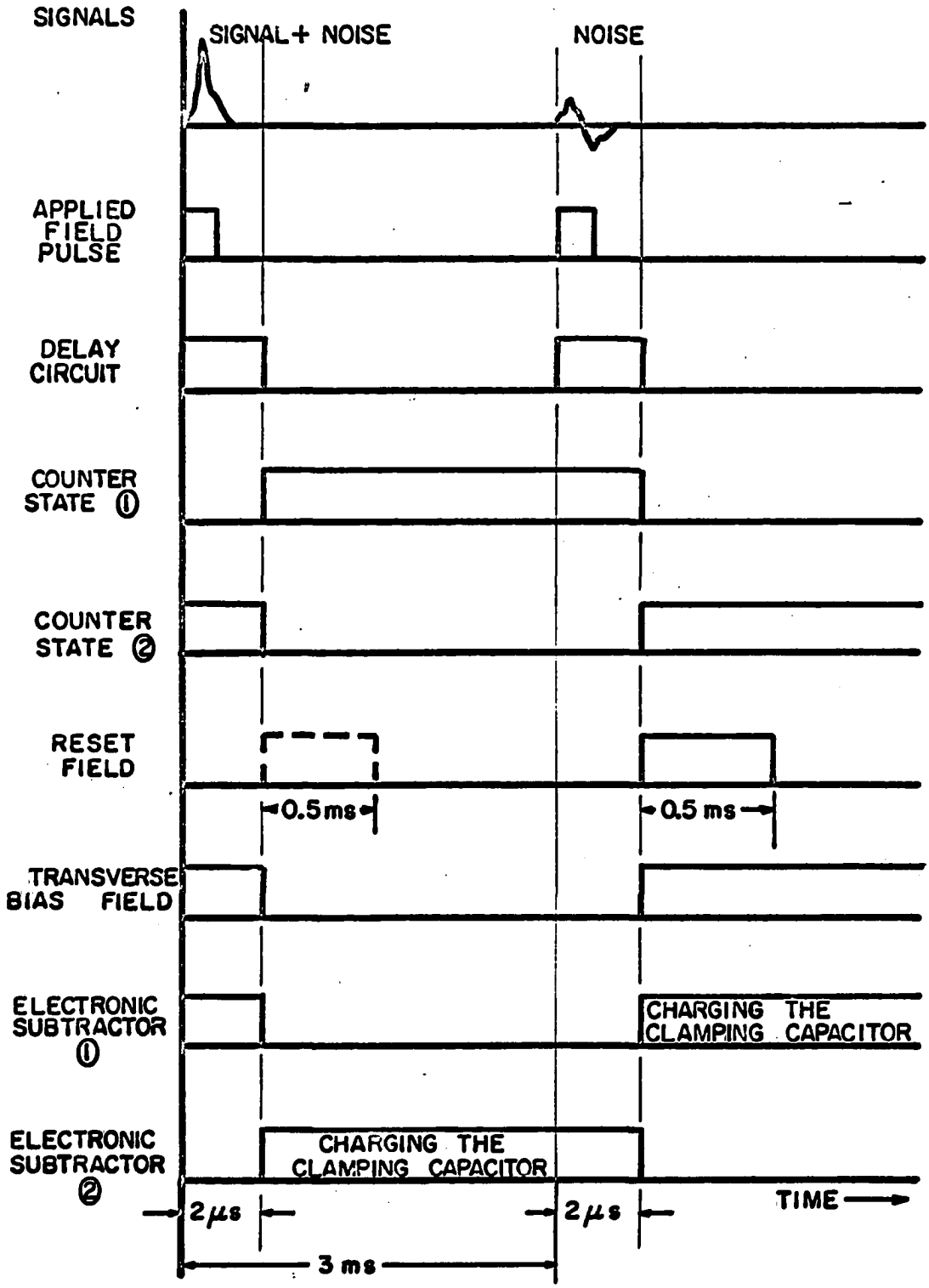

Fig. 13. Time sequence of logic operations and applied fields

III. EXPERIMENTAL RESULTS

A. Introduction

The purpose of the experimental work was to investigate magnetization reversal for thin, permalloy films with applied fields near the threshold for rotational switching. (See Appendix B) The apparatus described in Chapter 2 was used for all of the pulse measurements. The specific things observed and measured were:

1. The shape of longitudinal and transverse voltage signals which were induced by flux changes during the magnetization reversal.
2. The switching times for the fast rotation.
3. The percentage of flux switched by fast rotation.
4. The trajectory of the net magnetization during reversal.
5. The reversibility of magnetization's motion.

Table 1 gives a summary of the parameters for the films that were extensively studied. The H_K, H_C, and thickness were measured by using a hysteresis-looper; the damping constant, α, by the "free oscillation method" as described by Wolf (7); the angular dispersion by the Torok technique (20). All films were $\sim$2 to 3mm in diameter and were deposited on glass microscope slides.

It will be seen later that the behavior of the magnetization during reversal varied drastically with increasing angular dispersion. The importance of this parameter was to give a measure of the magnetization's non uniformity--the ripple amplitude, wave length, and orderliness. (6,9) Note also that the loss or damping increased with increasing dispersion which is in agreement with Nelson. (21)

Table 1. Measured magnetic thin film parameters

Magnetic Film No.	H_K oersted	H_c oersted	t angstrom	α dimensionless	α_{90} degrees
1	3.2	1.5	∿1000	.008	2
2	4.1	2.3	∿1000	.009	4
3	2.8	1.7	∿1700	.010	8
4	2.2	2.5	∿1000	.018	15

H_K - uniaxial anisotropy

H_c - coercive force for wall motion

t - thickness of the film

α - phenomenological damping constant for Gilbert's rotation model

α_{90} - angular dispersion (Torok)

B. Longitudinal and Transverse Voltage Wave Forms (LVW,TVW)

With a steady field applied in the hard (transverse) direction, H_T, and a pulse field in the easy (longitudinal) direction, H_L, the resulting magnetization flux changes were measured. Fig. 14 shows the LVW and TVW for film 1, with applied fields slightly greater than those needed for rotational switching. The large initial peak predicted by all models except the spin-wave model was due to the small damping coefficient. Because of the large torque, the magnetization rotated very rapidly when the longitudinal field was first applied. As it continued to rotate, the magnetization went through a torque minimum (see torque curves for H_L = 1.32 oe and 2.0 oe of Fig. 10 in reference (4)) slowing down and then speeding up again. This fluctuation caused the notched wave form. For

Fig. 14. The longitudinal (LVW) and transverse (TVW) voltage wave forms for film 1 - H_T = .52 H_K, H_L = .27 H_K - 1 nsec/cm, 10 mv/cm

Fig. 15. The longitudinal voltage wave forms for film 1 - H_T = .5 H_K, H_L = .2, .3, .4, .5, 1 H_K - 1 nsec/cm, 100 mv/cm

Fig. 16. The longitudinal voltage wave form for film 4 - H_T = .5 H_K, H_L = .5, .75, 1.0, 1.25, 1.5, 1.75, 2.0 H_K - 1 nsec/cm, 100 mv/cm

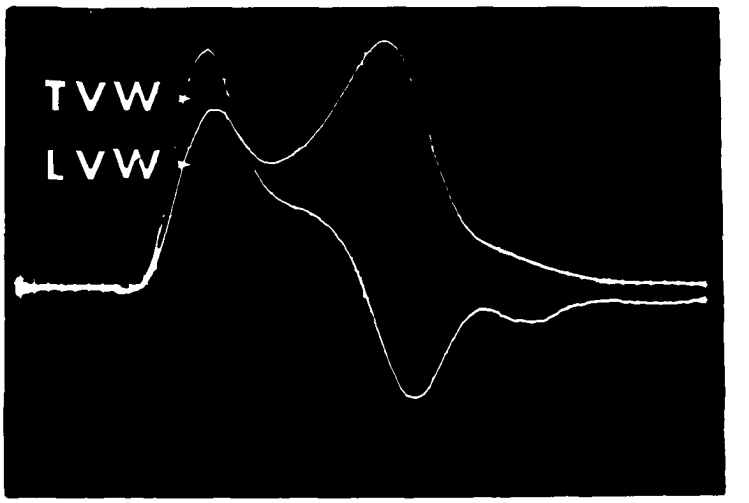
TVW
LVW

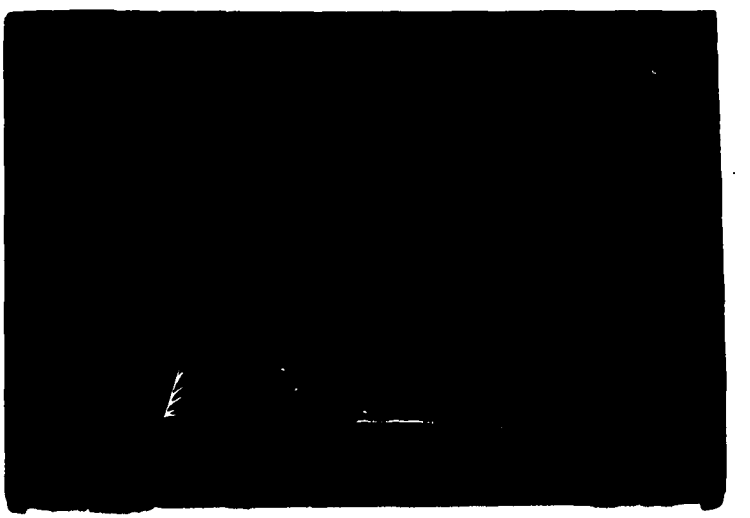

larger damping constants the magnetization responded more slowly, thus making the notch more and more shallow. This was seen experimentally.

In Fig. 14 the anomalous behavior was the lack of oscillations after the main voltage peak as would be expected with the film's small damping parameter. There was instead a long tail which is especially noticeable on the TVW. The behavior was as if the damping constant had increased by a factor of about 3 after ~75% of the flux had switched.

The LVW's for film 1, the low dispersion film, and film 4, the high dispersion film, are shown in Fig. 15 and 16 respectively. A steady transverse field one half their respective H_K's was used while varying the longitudinal field. Note the initial peak still exists, but the notch is highly attenuated for film 4 with the large α.

The wave forms differ greatly between the two films. For film 1 the time lapse from the application of the longitudinal field pulse to the main peak of the LVW decreased with increasing fields. As the dispersion increased, the time lapse varied less until it was approximately a constant with film 4. The switching times discussed later show this fact very clearly. (See Fig. 21) Also note how it takes a much higher relative field to switch film 4 than to switch film 1.

C. Switching Times for Fast Rotation

Measurements were made to determine switching times for fast rotation versus applied fields. The criterion used was the following:

> the time interval between the 20% points of the longitudinal voltage wave form's maximum height was by definition the switching time for fast rotation.

This particular criterion was chosen for many reasons:

1. Ease with which the measurement could be made.

2. "Noise" due to oscillations of the magnetization which gives erroneous results was avoided.

3. As seen in Figs. 14 and 22, there is a long tail following the maximum voltage peak for small spplied fields. By using a criterion of 10%, as in Fig. 1, this tail which was not considered as part of of the fast rotation was at times included in the switching speed.

Essentially, the switching speed measurement was based on the Gilbert model where the LVW sharply drops to approximately zero after reaching its maximum value. (See Fig. 41) Any deviation from these switching signals could no longer be classified as fast rotation a la Gilbert and therefore, anomalous. Because this criterion separated the "fast from the slow", it was possible to measure the amount of flux which switched by fast rotation. Further discussion of the flux measurement will appear in the next section.

The major disadvantage in using the 20% criterion was its dependence on the rise time of the sense system.

The results for the four films are shown in Figs. 17, 18, 19, and 20. For small H_T the effects of dispersion are very apparent. One way to visualize this effect is to consider the film as consisting of many regions with the magnetization skewed due to variations of anisotropy field, etc. If H_T was too small, some of the magnetization would not have had its direction in the same quadrant of the transverse field (i.e., some would have negative ϕ values, Fig. 3). Consequently, when the longitudinal field was initially applied, not all parts of the film would rotate in the same direction. Because of magnetostatic coupling, the overall process would

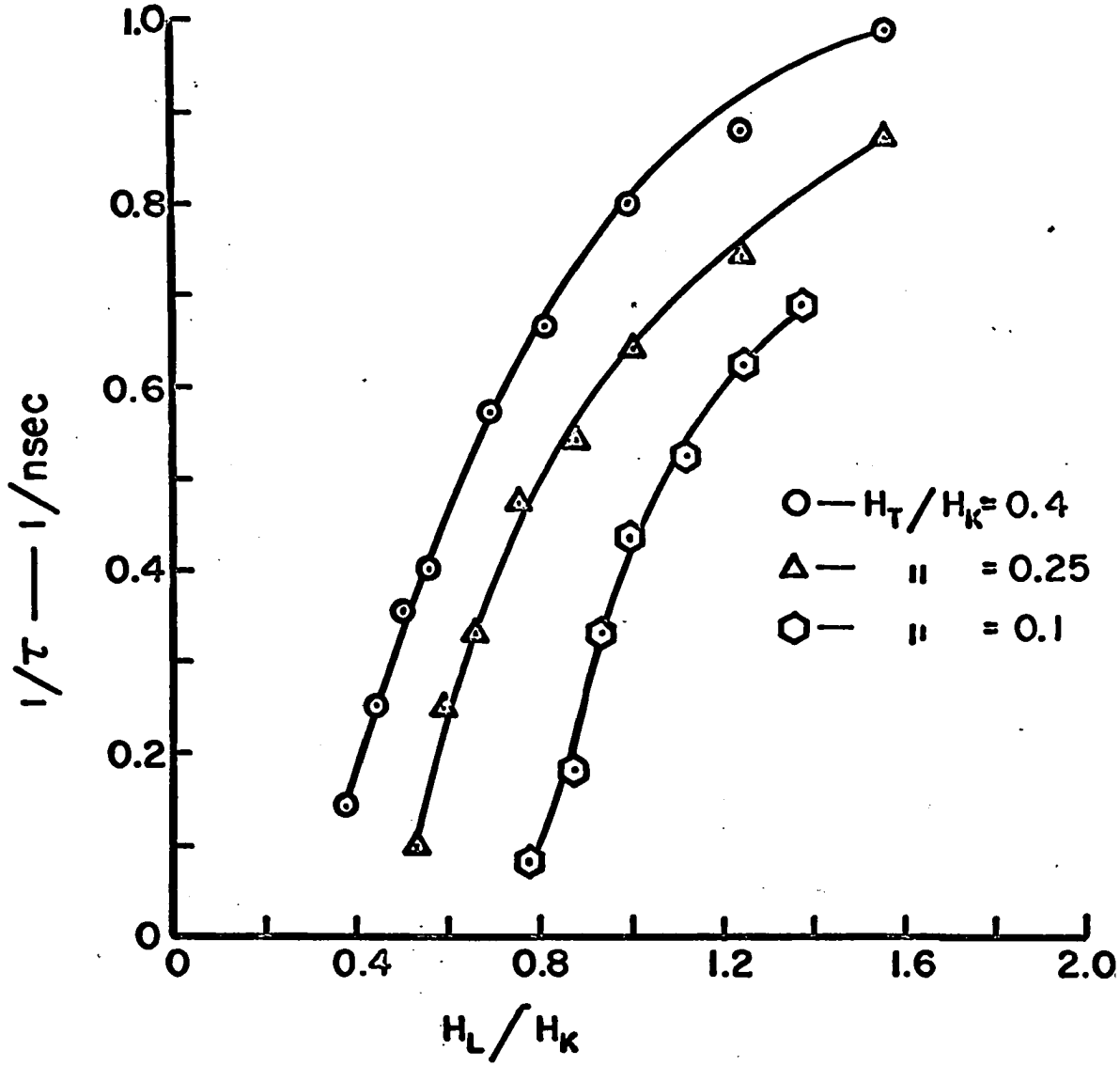

Fig. 17. Fast rotation inverse switching times, $1/\tau$, versus normalized applied fields, H_L/H_K and H_T/H_K, for film 1.

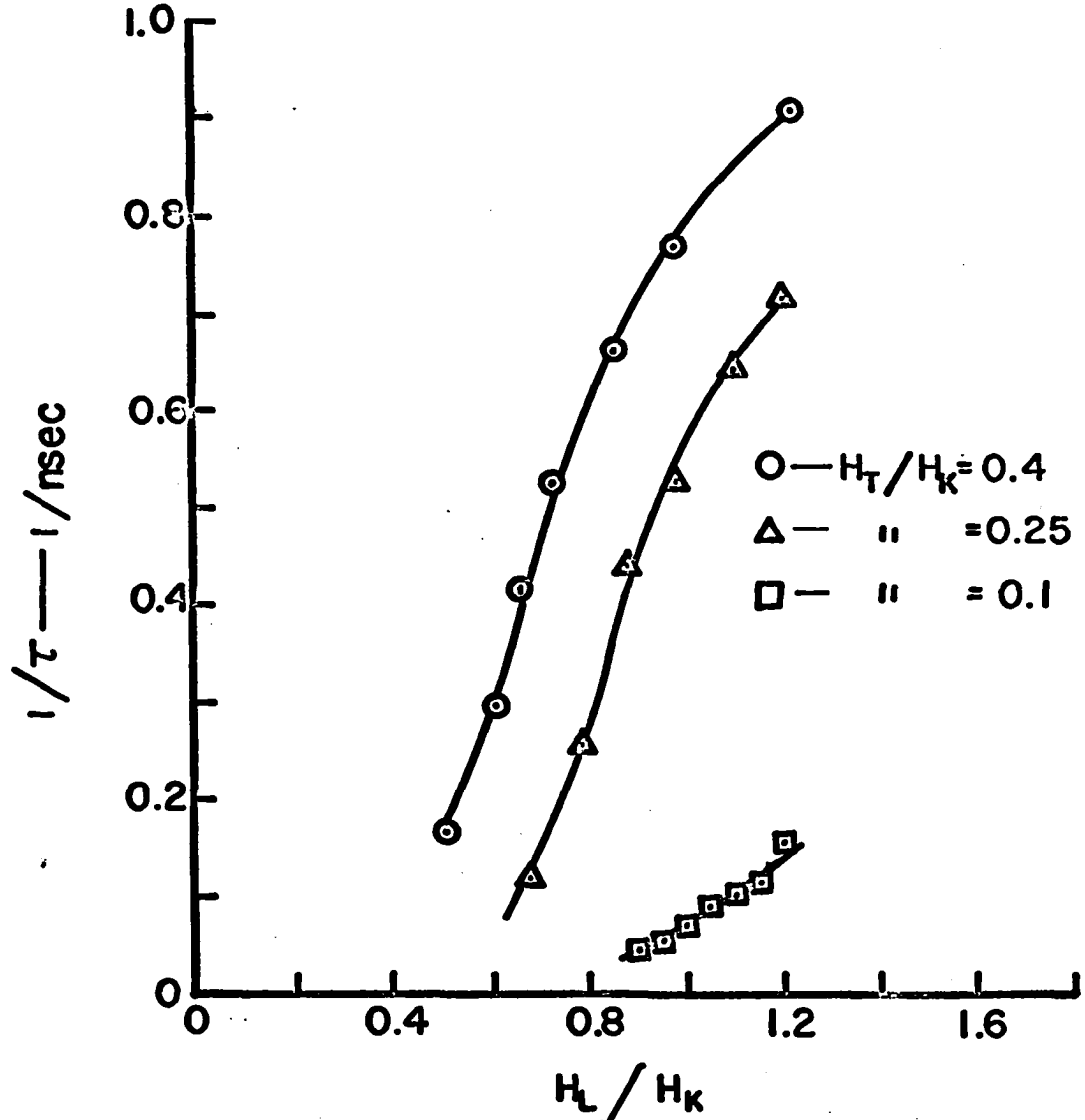

Fig. 18. Fast rotation inverse switching times, $1/\tau$, versus normalized applied fields, H_L/H_K and H_T/H_K, for film 2

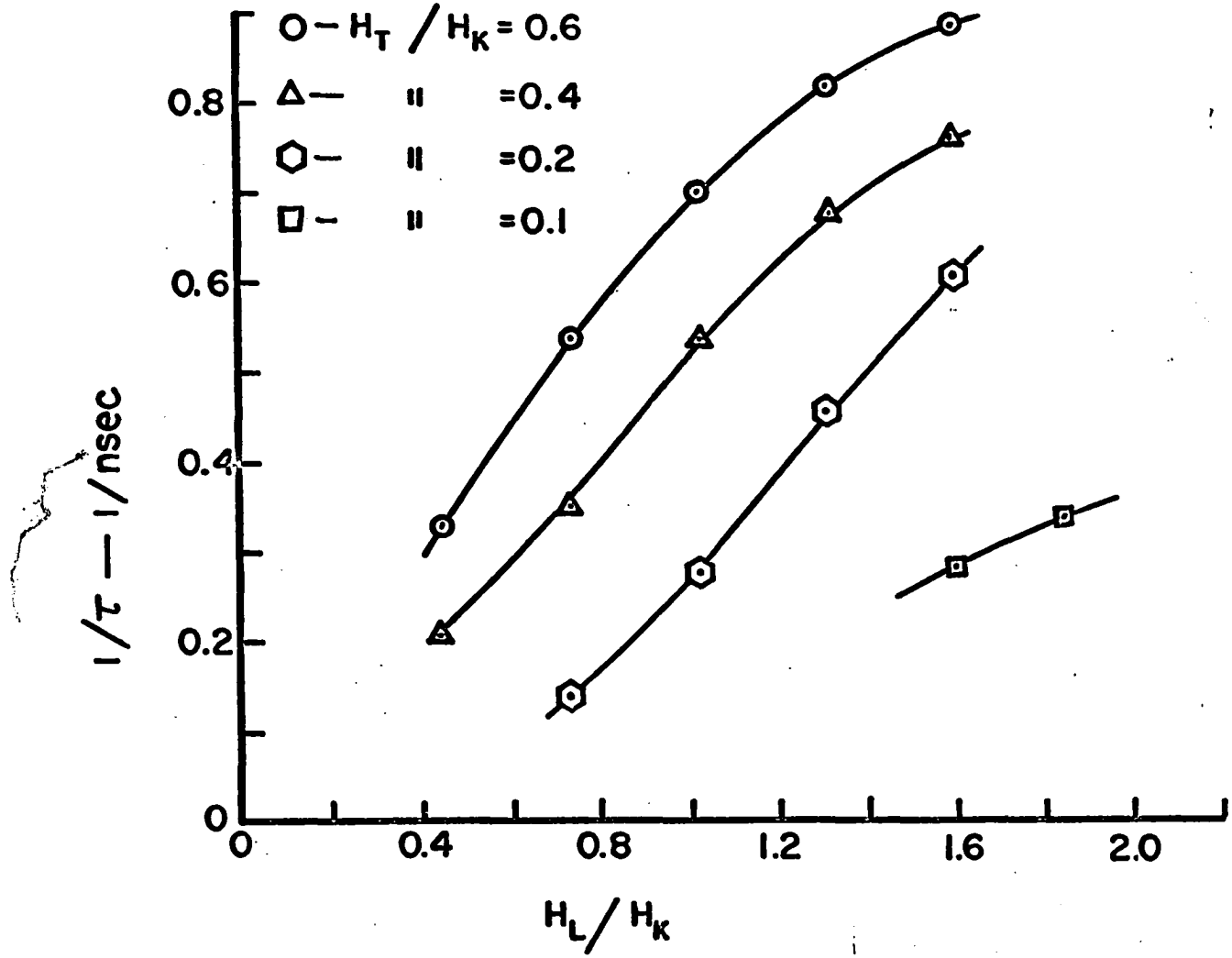

Fig. 19. Fast rotation inverse switching times, $1/\tau$, versus normalized applied fields, H_L/H_K and H_T/H_K, for film 3

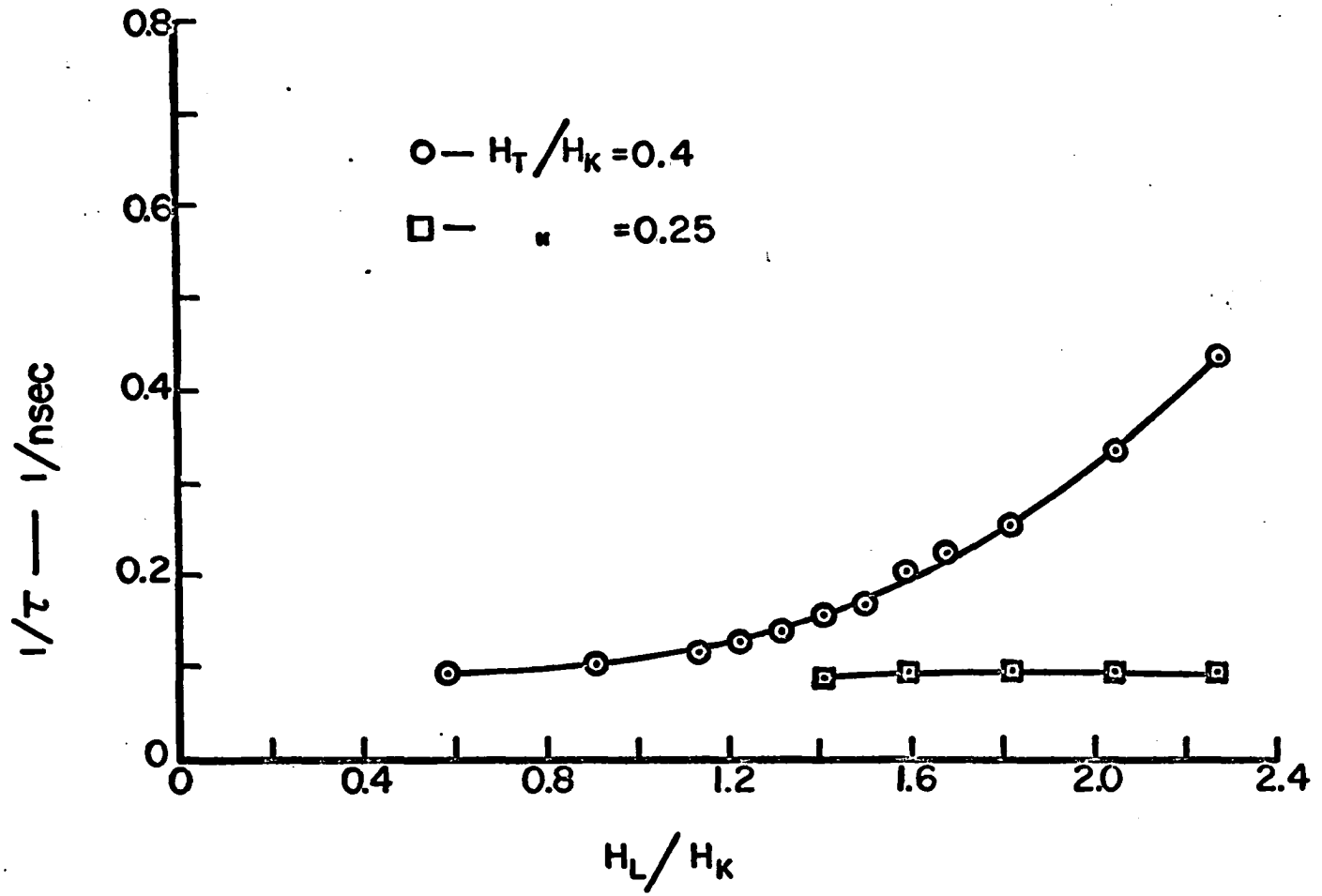

Fig. 20. Fast rotation inverse switching times, $1/\tau$, versus normalized applied fields, H_L/H_K and H_T/H_K, for film 4

seem to be slower and, as will be seen from flux measurements, would not switch entirely by fast rotation. This showed up experimentally when the slope of the switching curves for a given film increased with H_T until the film was rotating more or less uniformly.

In Fig. 21 the composite results for $H_T = .4\ H_K$ are plotted. With this size bias all parts of even the most dispersive film should be rotating in the same direction. Even so, there was a large disparity in switching times which can not be attributed to the film's various damping constants. Generally, the greater the dispersion, the greater the variation both in curvature and slope. This observation would be expected considering the drastic differences in LVW as shown in Figs. 15 and 16.

D. Flux Switched by Fast Rotation

By integrating LVW with a analog computer as it comes out of the noise reducer, the flux change in the longitudinal direction was obtained. Or since

$$V_L = \frac{K_L dM_L}{dt}$$

then

$$M_L(t) = M_L(0) + \frac{1}{K_L} \int^{t} V_L(X)dX$$

where

M_L--net magnetization in the longitudinal direction

K_L--a constant depending on sense coil and film geometry

V_L--longitudinal voltage.

The integral has a limit as $t \to \infty$, $M_L(\infty)$ (i.e., the film has completely switched). Since the initial and final angle of the magnetization depends

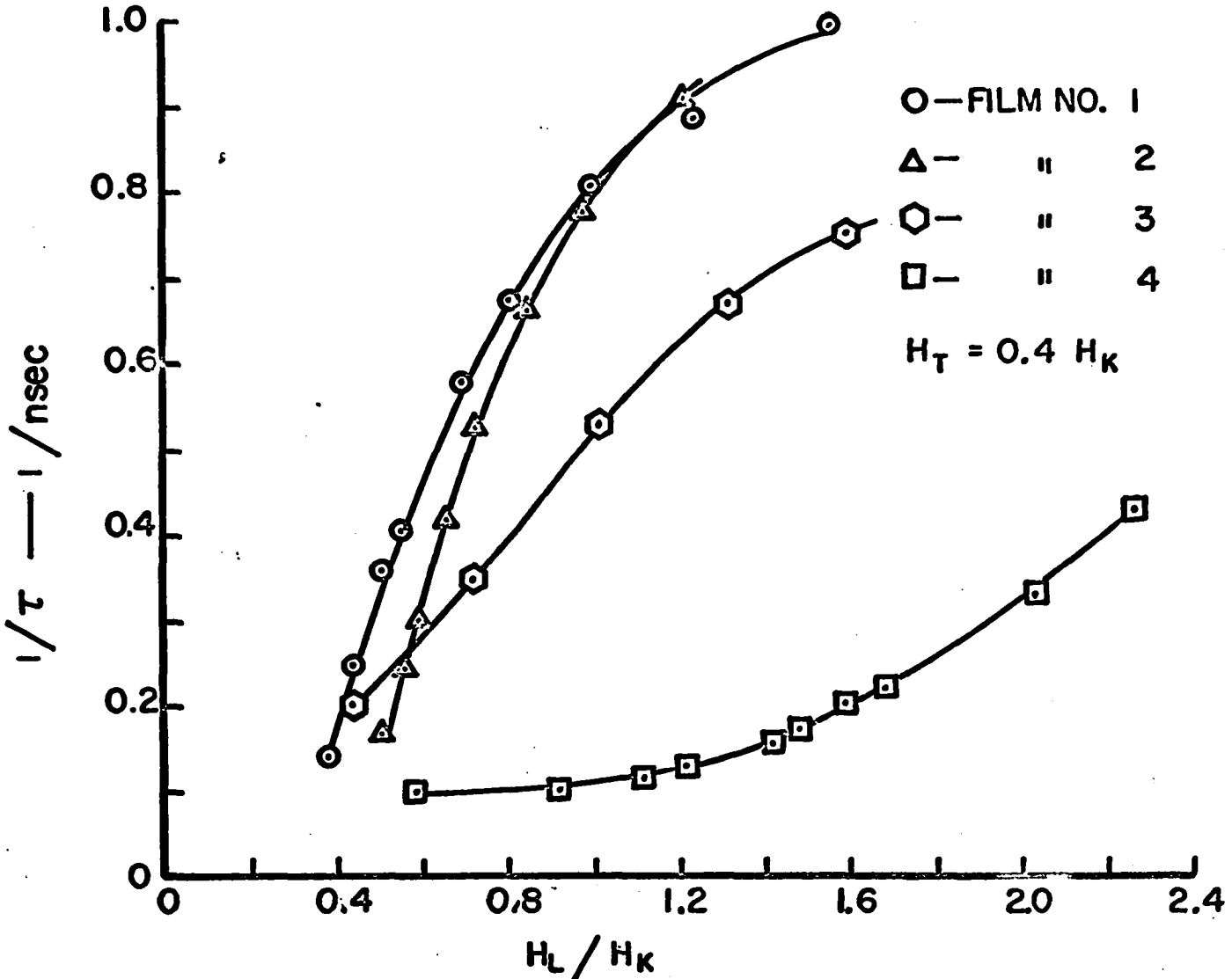

Fig. 21. Composite inverse switching times for fast rotation, $1/\tau$, versus normalized applied field, H_L/H_K, where $H_T = .4\ H_K$

on the applied field, so do $M_L(0)$ and $M_L(\infty)$. Fig. 22 displays the LVW's and their corresponding integrals for film 2.

For these measurements the value of the integral was recorded when the LVW dropped to 20% of its maximum amplitude, t_f. The integral then gave the amount of flux (or magnetization) that was reversed by fast rotation. The problem was to properly normalize the measured integrated voltages. By applying a sufficiently large longitudinal pulse field, the integral reached a maximum or saturated value within 5 to 10 nsec. The saturation assured that the film was reversing completely by pure rotation. Because of the criterion used for the fast switching, the integral measured at t_f was slightly smaller than the saturated value. Then the following relation was used to find the proportionality factor, K:

$$K = \frac{\left|\text{the theoretical value of } M_L(0) - M_L(\infty)\right|}{\left|\text{integral of the LVW up to } t_f\right|} ,$$

thus solving the problem.

When the longitudinal field was reduced, the part of the flux that switched by fast rotation, ΔM_F is

$$\Delta M_F = K \frac{\left|\text{integral of the LVW up to } t_f\right|}{\left|\text{the theoretical value of } M_L(0) - M_L(\infty) \text{ for the given applied fields}\right|} .$$

The ΔM_F versus applied field for the four films is plotted in Figs. 23, 24, 25, and 26. They show several interesting aspects of flux reversal. One is, as many authors have noted, that magnetization does <u>not</u> switch purely by rotation when the fields slightly exceed those predicted by

Fig. 22. Longitudinal voltage wave forms and their corresponding integrals for film 2

a. $H_T = .25\ H_K$, $H_L = .72, .86, .95, 1.07, 1.20$ .5 nsec/cm

Top - integrals, .45 $|\overline{M}|$/cm

Bottom - LVW, .05 V/cm

b. $H_T = .25\ H_K$, $H_L = .62, .67, .72\ H_K$ 2 nsec/cm

Top - integrals, .09 $|\overline{M}|$/cm

Bottom - LVW, .01 V/cm

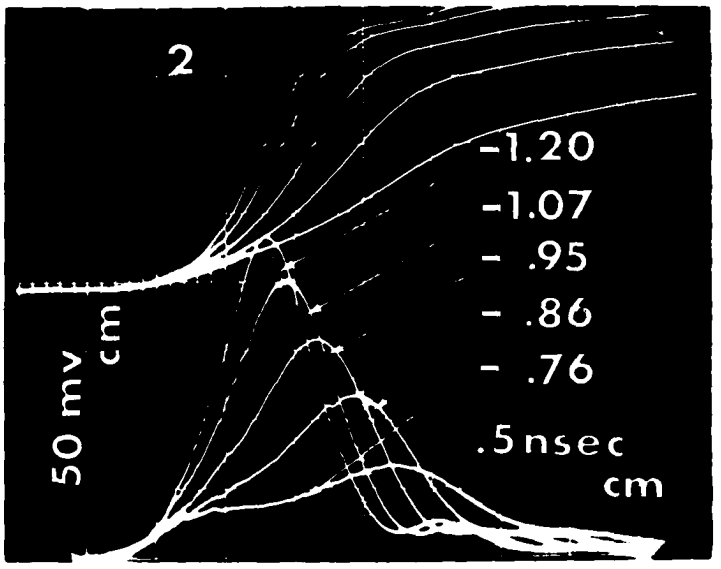
2
-1.20
-1.07
- .95
- .86
- .76
.5nsec
cm
50 mv
cm

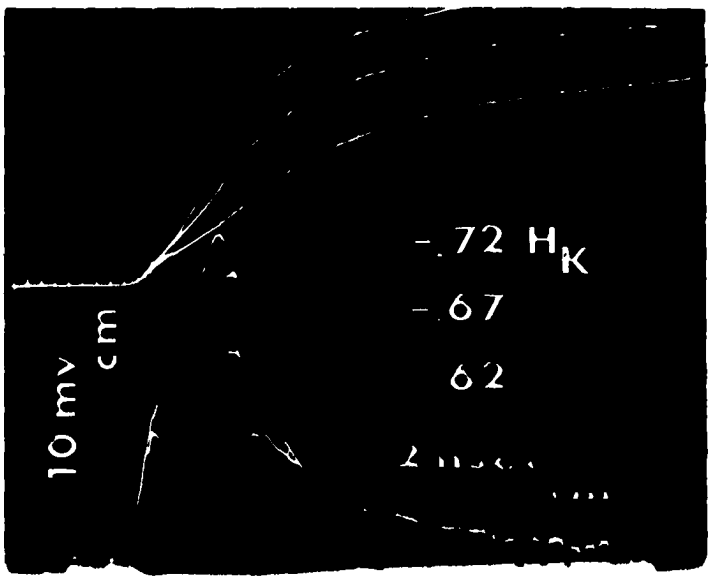
-.72 H_K
-.67
62
10 mv
cm

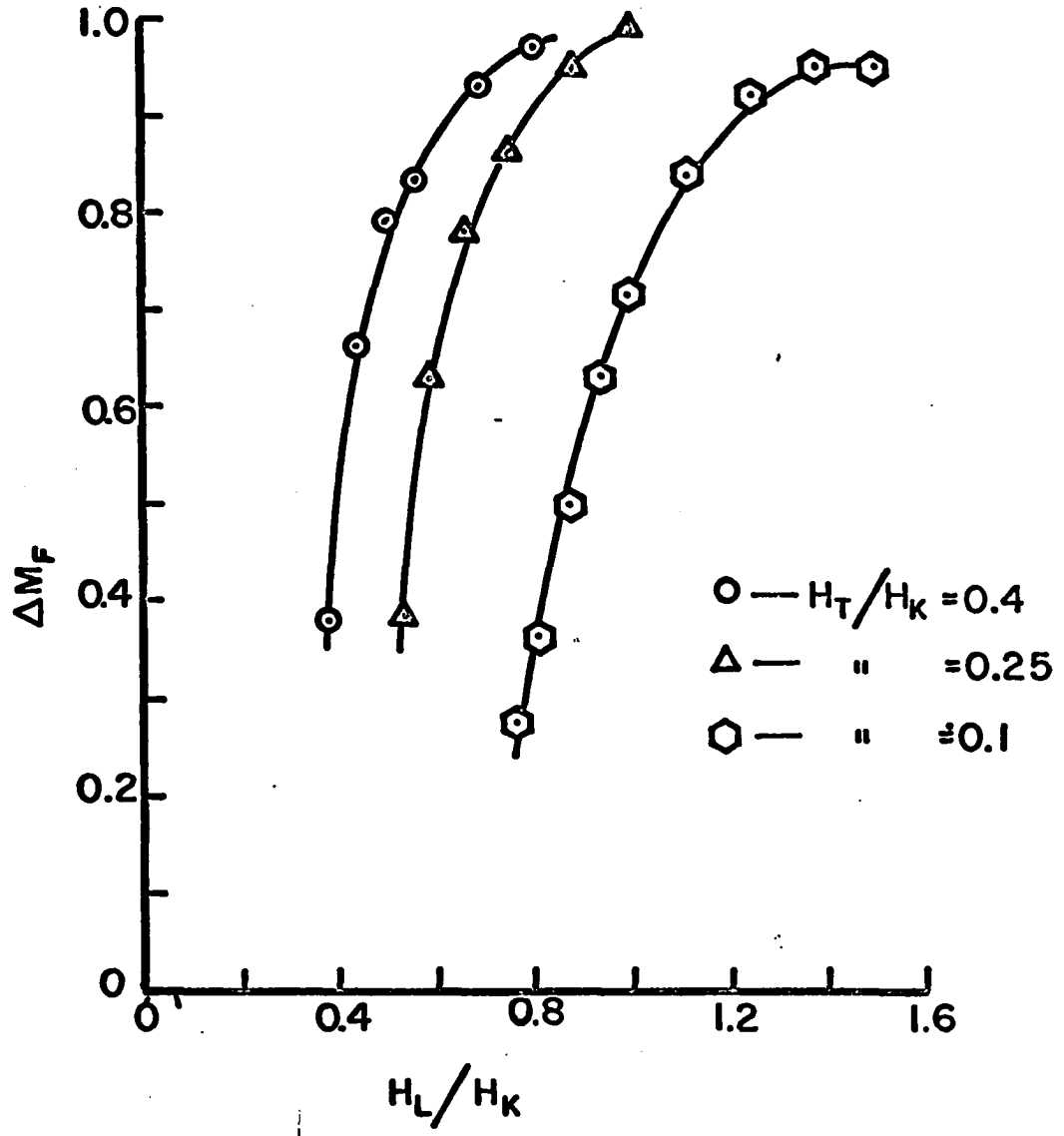

Fig. 23. Flux switched by fast rotation, ΔM_F, versus applied normalized fields, H_L/H_K and H_T/H_K, for film 1

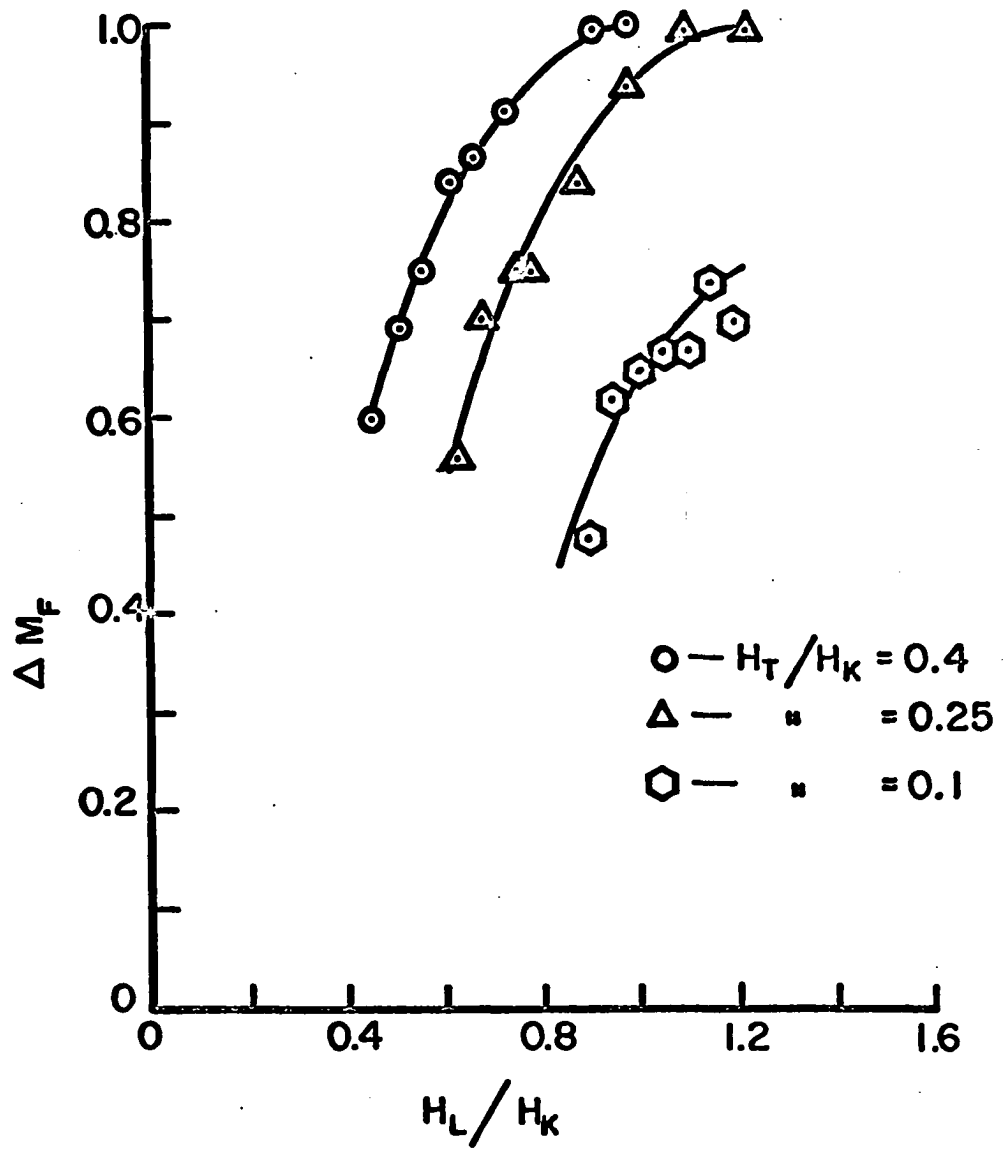

Fig. 24. Flux switched by fast rotation, ΔM_F, versus applied normalized fields, H_L/H_K and H_T/H_K, for film 2

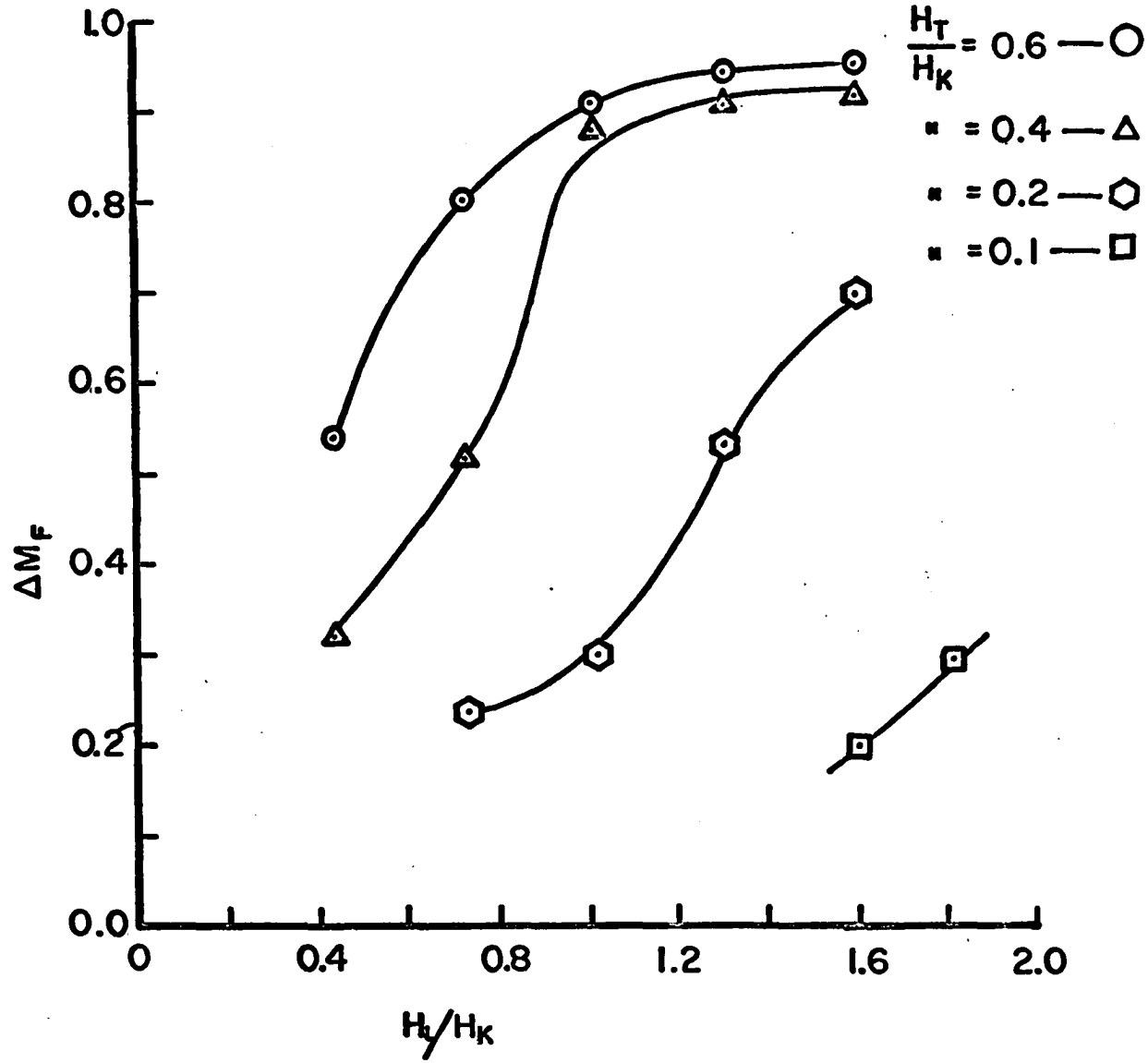

Fig. 25. Flux switched by fast rotation, ΔM_F, versus applied normalized fields, H_L/H_K and H_T/H_K, for film 3

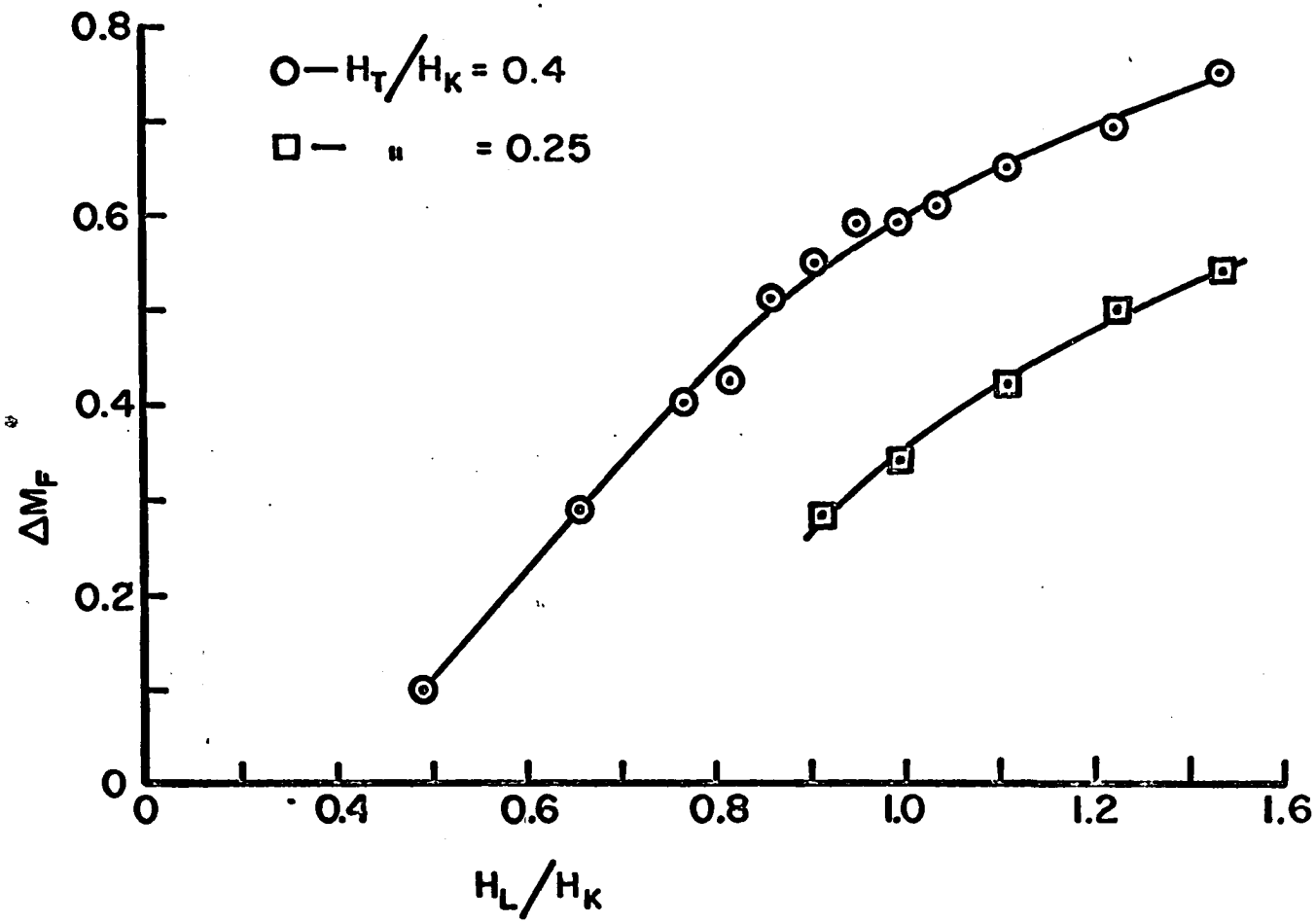

Fig. 26. Flux switched by fast rotation, ΔM_F, versus applied normalized fields, H_L/H_K and H_T/H_K, for film 4

Stoner-Wohlfarth. As the dispersion increases, this type of reversal becomes more difficult as is illustrated in Figs. 27 and 28. Fig. 27 is a composite of ΔM_F for the various films under similar transverse biasing. Fig. 28 are the fields needed to switch 50% of the flux by fast rotation with respect to the Stoner-Wohlfarth critical fields.

The next point of interest is that ΔM_F is a smooth continuous function of applied field. Hence, there is not sharp threshold for rotationl switching. However, as the dispersion decreases, the slopes of the curves get steeper, thus showing again the effects of nonuniformity.

There seem to be several possible reasons for the slope dependence.

1. For low applied fields, only the portions of the film with low H_K values reverse leaving unswitched areas. Subsequent reversal of the entire film would proceed more slowly by the motion of the walls formed between the two regions.

2. The magnetization rotates uniformly, but somehow stops or locks up at various angles. The "somehow" is the basis of the work by Harte (6) and Stein (14).

3. Because of the high stray fields at the boundary of the film, the magnetization tends to be locked and unswitchable for moderate fields. (22) If only the center portion of the film reversed, higher demagnetizing fields would result which could skew the magnetization at various angles.

For these measurements the third possibility can pretty well be discarded for the following reasons:

a. Circular films were used, thus reducing edge effects.

b. The Kerr patterns made by Stein (14) show large volume effects.

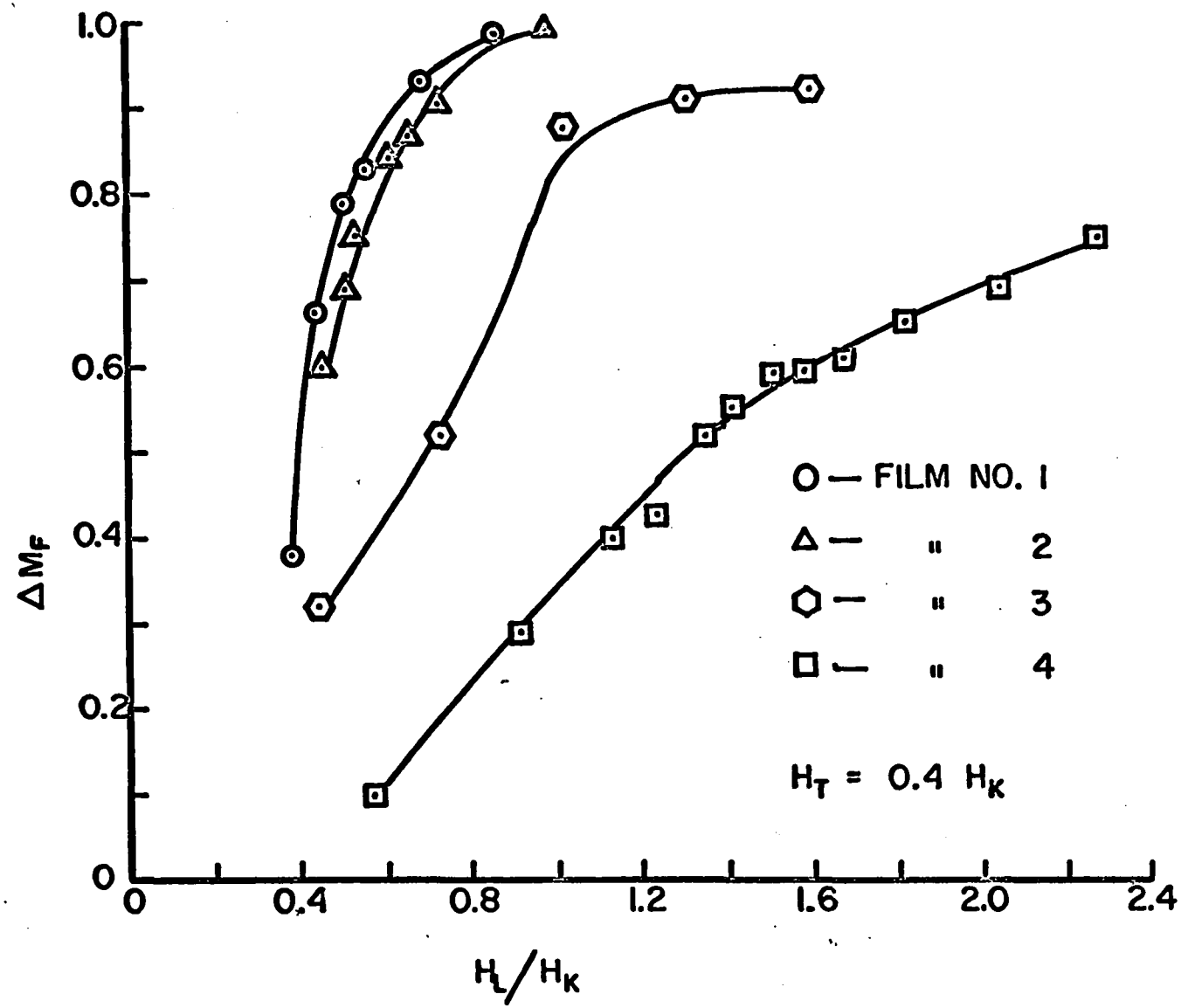

Fig. 27. Composite of flux switched by fast rotation, ΔM_F, versus applied normalized field, H_L/H_K, with $H_T = .4\ H_K$

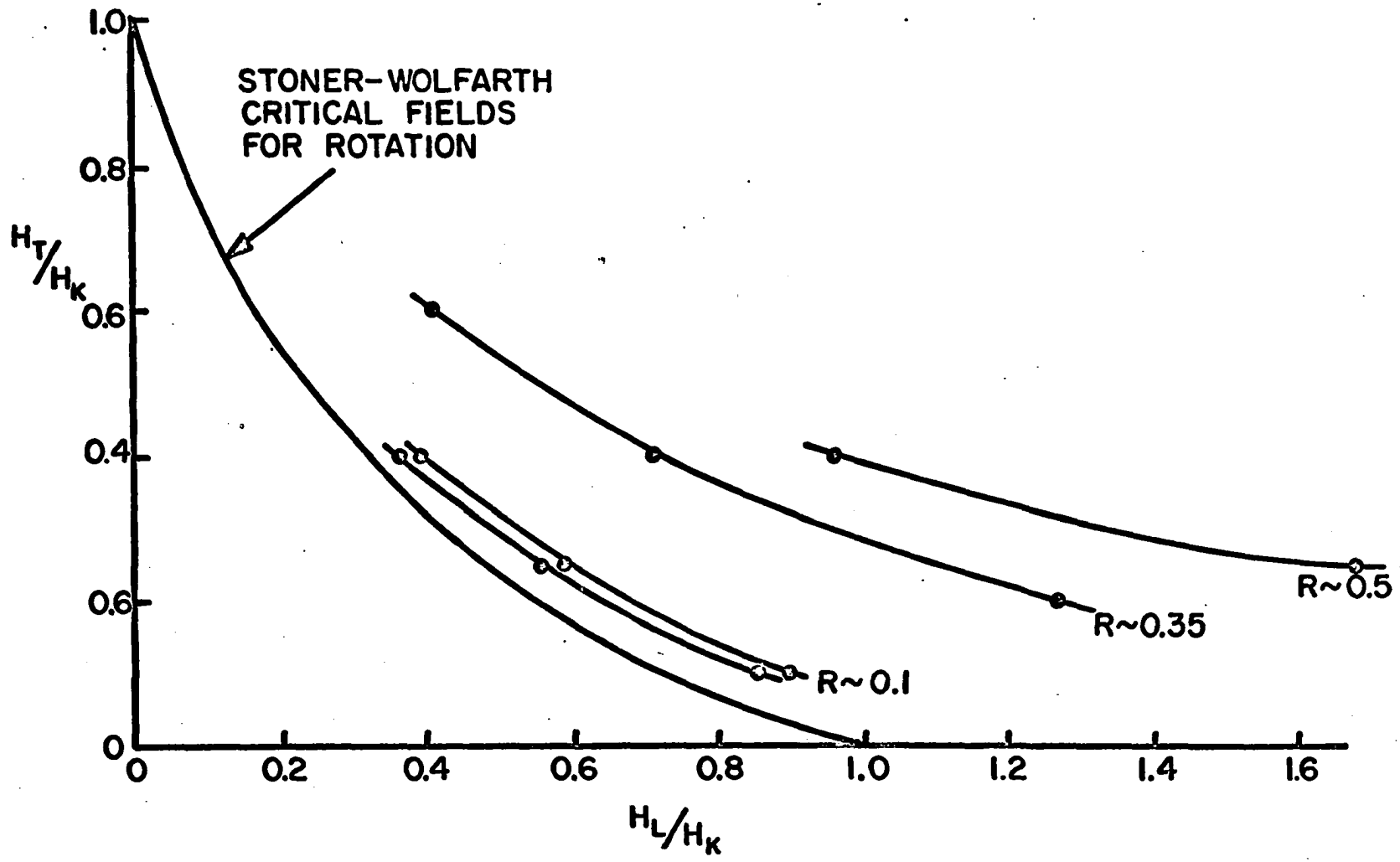

Fig. 28. Plot of normalized applied fields, H_L/H_K and H_T/H_K to switch 50% of the flux by fast rotation
R - spin-wave reaction torque parameter

In this thesis bitter patterns were used and they substantiate Stein's findings. (See page 60)

To prove the feasibility of the remaining possibilites, further evidence is needed. (See next section)

E. Trajectories of the Magnetization

By integrating both the LVW and TVW with the aid of an analog computer, the longitudinal and transverse flux, $M_L(t)$ and $M_T(t)$, were obtained. But

$$\bar{M}(t) = M_L(t)\,\bar{a}_L + M_T(t)\,\bar{a}_T$$

$\bar{M}(t)$---net magnetization

$\bar{a}_L$ ---longitudinal direction unit vector

$\bar{a}_T$ ---transverse direction unit vector

Consequently, by adding $M_L(t)$ and $M_T(t)$ at "right angles", $\bar{M}(t)$ was obtained. This was done by driving the vertical and horizontal amplifiers of an oscilloscope with $M_T(t)$ and $M_L(t)$ respectively. The result was the "trajectory of the magnetization".

If rotational switching was the only mechanism, the trajectory would be a circular arc ($|\bar{M}|$ = a constant) as seen in Fig. 29. The effect of the sense system's finite band pass was to distort the trajectories. Fig. 30 shows the theoretical result using the "filtered" (Chapter 4) Gilbert's model with film 1 parameters, $H_T = .5H_K$ and $H_L = .5H_K$. The oscillations were due to the magnetization overshooting its equilibrium position. (See Fig. 15)

Because the induced anisotropy tries to keep $\bar{M}$ parallel (or anti-parallel) to the easy axis, it resists the rotation of the magnetization for $\phi < 90°$ and aids reversal for $\phi > 90°$. Therefore, the angular

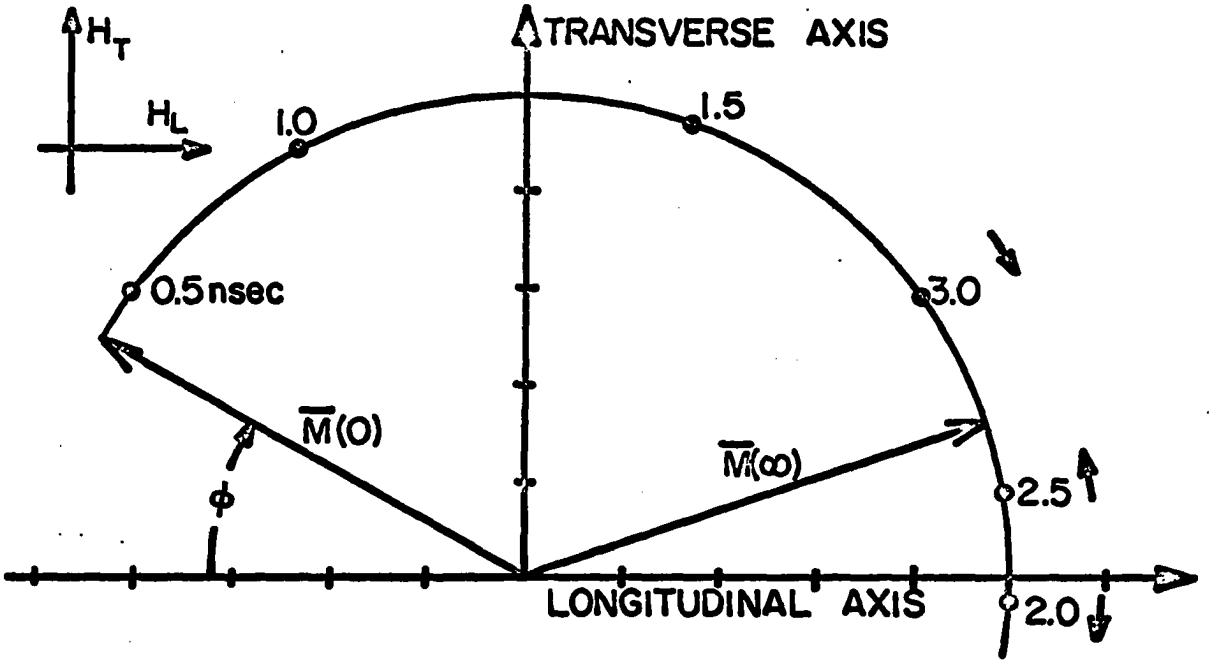

Fig. 29. Theoretical trajectory of the magnetization for the rotation model, film 1 parameters, $H_T = H_L = .5\ H_K$

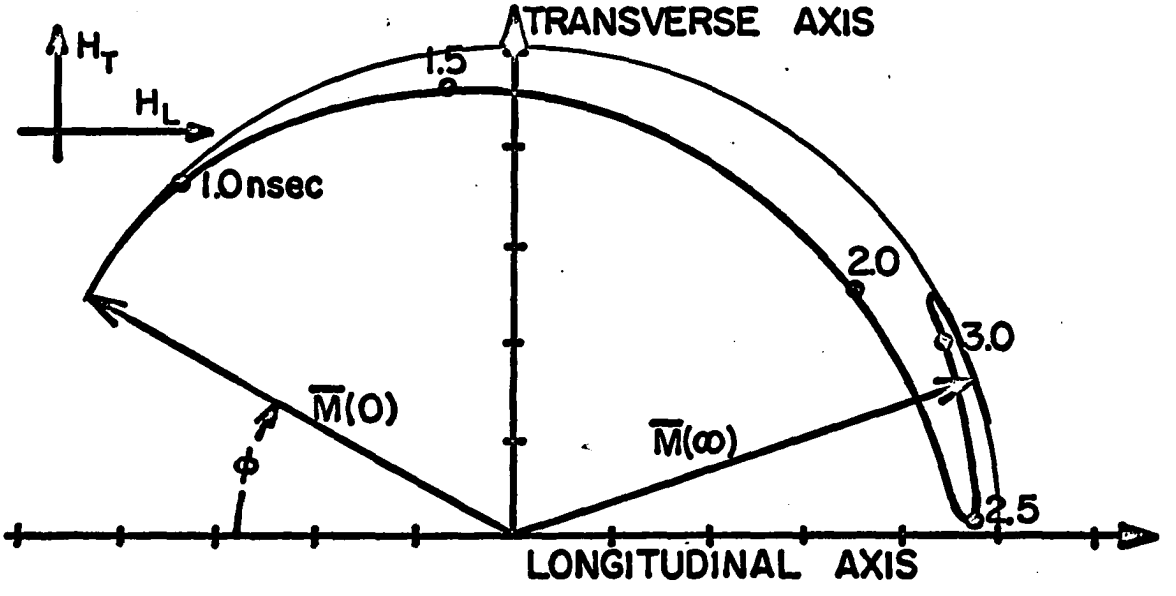

Fig. 30. Theoretical trajectory of the magnetization of Fig. 29

velocity, $\frac{d\phi}{dt}$ should be much larger in the second quadrant than the first. This is evident from Fig. 30 where the larger the deviation from a circular arc, the faster the rotation. (From pure rotation computer solutions it may take $\overline{M}$ 5 nsec to rotate to 90° and then .5 nsec to reach its final switched equilibrium angle.) If $\overline{M}$ does not speed up in the second quadrant but instead slows down, this anomalous behavior will be called locking. It can be quantitatively found; for, the M_L value where locking occurs is just ΔM_f. All this background information is presented in an attempt to give the reader a better appreciation for the following results.

The trajectory measurements were made 1) for small transverse bias fields where the curve of the inverse switching time versus applied field is flat, Fig. 18, and 2) for large bias fields where the pure rotation model was expected to hold.

Fig. 31 shows the results for film 2 for H_T = .1 H_K = .85, .9, .95, 1.0 H_K with a total integration time of 50 nsec. The "o's" denote the points where ΔM_f occurs on the trajectory. Here $|\overline{M}|$ was not conserved as shown by the trajectories' asymmetry about the hard axis; $|\overline{M}|$ in the second quadrant was smaller than in the first. This is consistant with wall formation. However, no conclusions can be made. Reversal for small transverse bias fields still requires further investigation.

For larger bias fields very interesting effects were observed. Some results are shown in Fig. 32 using film 2 with H_T = .4 H_K, H_L = .46, .51, .56, 1.1 H_K and integrating over 50 nsec. Here the situation was very much different than with small H_T; $|\overline{M}|$ approximately equaled a constant until locking. This was confirmed by greatly magnifying the trajectories

Fig. 31. Trajectories of the magnetization using small H_T for film 2

$H_T = .1\ H_K$, $H_L = .85, .9, .95, 1.0\ H_K$

50 nsec - total integration time

o - denotes locking

• - ideal trajectory

Fig. 32. Trajectories of the magnetization using large H_T for film 2

$H_T = .4\ H_K$, $H_L = .46, .51, .56, 1.1\ H_K$

50 nsec - total integration time

o - denotes locking

• - ideal trajectory

Fig. 33. Trajectories of the magnetization for the high dispersion film 4

$H_T = .5\ H_K$, $H_L = .5, .75, 1.0, 1.5, 1.75, 2.0\ H_K$

20 nsec - total integration time

o - denotes locking

• - ideal trajectory

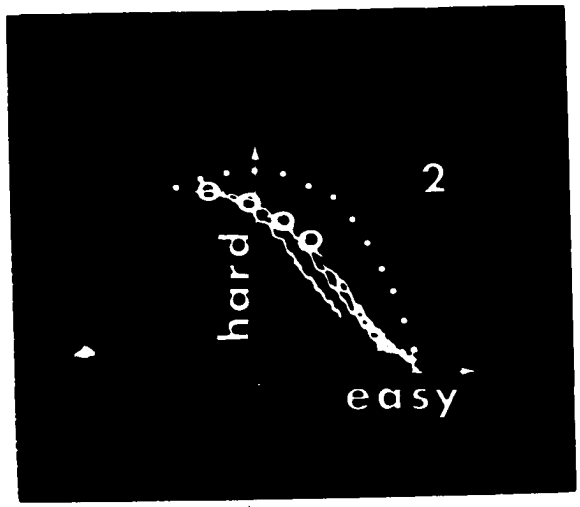
2
hard
easy

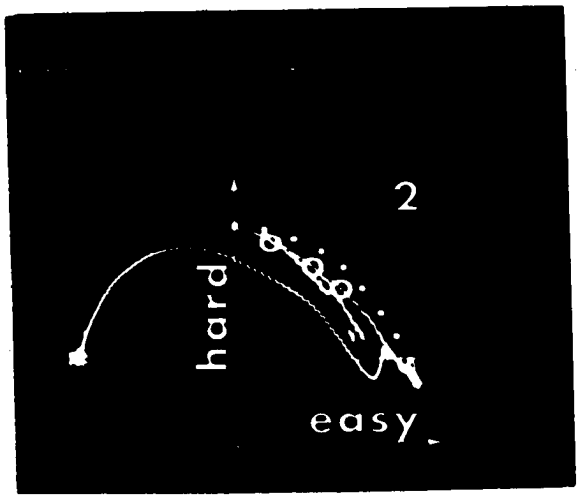
2
hard
easy

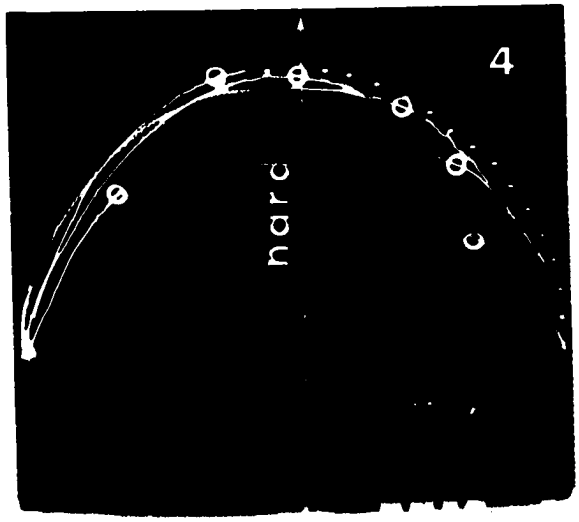
4
narc

during the first quadrant of switching. Up to $\phi = \frac{\pi}{2}$ they were found to coincide with each other to within 3% (experimental error). Once locking occurred, $|\overline{M}|$ decreased. The important thing to note is that locking can occur in the second quadrant where the angular velocity of $\overline{M}$ should, according to the spin-wave and pure rotation models, be the greatest. (A measure of the angular velocity is the intensity of the oscilliscope trace. When $\overline{M}$ moves rapidly, the trajectory is faint and/or consists of "steps". If instead it is very luminous, $\overline{M}$ is traveling at a slow rate.) Another example, Fig. 33, is shown for film 4. The trajectories were found to become more circular as the dispersion increased.

The fields needed to slow down the rotation would have to be approximately equal to the ones that were aiding the switching of the magnetization (fields on the order of 5 oe, depending on the particular film). Such a large field was not likely to come from either:

1. Trapped flux in the center conductor, since the films were on 5 mils glass.
2. Or edge effects, because the samples were circular and large (3 mm in diameter). If edge effects were responsible, the trajectories would not have overlapped as with film 2.

In the author's opinion, instabilities are the only way to explain this phenomenon. In Chapter 4 it is shown that the resulting fields from instabilities are indeed large enough to cause such behavior. However, further evidence is needed to show that such changes in the magnetization can occur in a few nanoseconds. This is done in the next section.

F. Reversability

Experiments were made where the longitudinal pulse ends before the switching of the magnetization was completed. If the pure rotation model (and perhaps the spin-wave model) were applied, the magnetization would be expected to either continue or reverse to its initial position with $|\overline{M}|$ remaining a constant.

These experiments proved that $\overline{M}$ was only reversable when the pulse ended before the notch appeared in the longitudinal wave form. This is demonstrated in Figs. 34 and 35 with the $M_L(t)$ shown in the top part of the photograph and the longitudinal signal in the lower. In Fig. 34 the applied fields were constant, but the duration of the pulse was changed. The reason the first parts of the wave forms did not perfectly coincide was because of the different characteristic impedances (50 to 55Ω) of the charge cables. The pulse length was kept constant in Fig. 35, but the amplitude of the longitudinal pulse was changed. For each field amplitude the wave forms and integrals are shown where a short and a long pulse were applied. In both cases note that the integral or $M_L(t)$ does not return to zero unless the pulse ends before the low point of the notch. The cause for the irreversability was attributed to instabilities in the magnetization which start to grow at that point.

With the short duration pulse field, the magnetization never continued rotating, even if it was at an angle greater than 90° with respect to the easy axis.

In Figs. 36 and 37 the magnetization first started to reverse itself, then collapsed within a few nanoseconds. The anomalous reversing was attributed to ripple patterns lagging behind net magnetization. The amount

Fig. 34. Reversability behavior versus pulse field duration for film 1

H_T = .25 H_K, H_L = .56 H_K, 2 nsec/cm

pulse width - 3 nsec, 5 nsec, 300 nsec

Toptraces - integral of bottom traces

Bottom traces - longitudinal voltage wave forms

Fig. 35. Reversability behavior versus pulse field duration for film 1

H_T = .4 H_K, H_L = .37, .41, .44 H_K, 2 nsec/cm

Top traces - integral of bottom traces

Bottom traces - longitudinal voltage wave forms

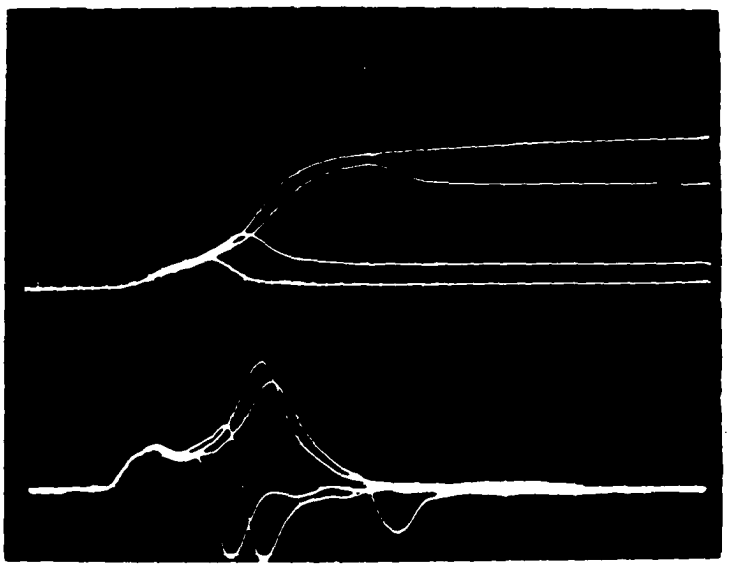

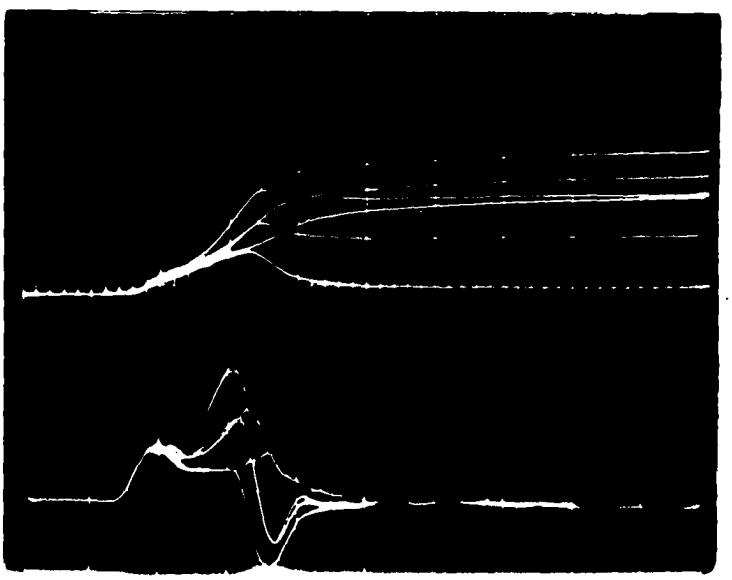

Fig. 36. Trajectories of the magnetization where the field pulse duration is shorter than the switching time for film 2

$H_T = .25\ H_K$, $H_L = .68, .73, .78, .88, 1.2\ H_K$

2 nsec - field pulse duration

20 nsec - integration time

o - denotes locking

Fig. 37. Trajectories of the magnetization where the field pulse duration is shorter than the switching time for film 4

$H_T = .5\ H_K$, $H_L = .9, 1.35, 1.8, 2.3\ H_K$

4 nsec - field pulse duration

20 nsec - integration time

o - denotes locking

Fig. 38. Trajectories of the magnetization where the pulse field is interrupted for 25 nsec for film 1

$H_T = .25\ H_K$, $H_L = .51, .55, .58\ H_K$

7 nsec - pulse duration up to interruption

50 nsec - integration time

o - denotes locking

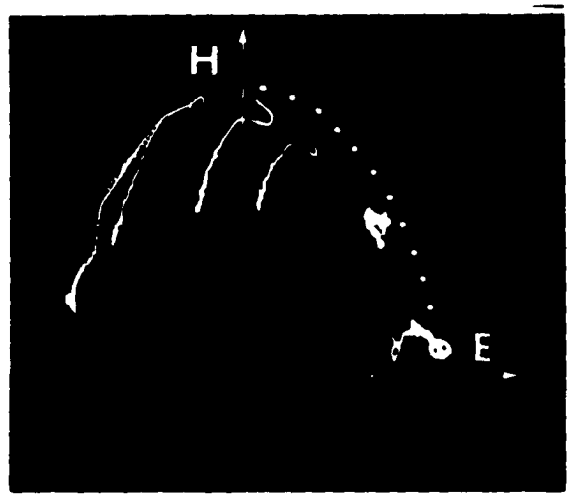
H
E

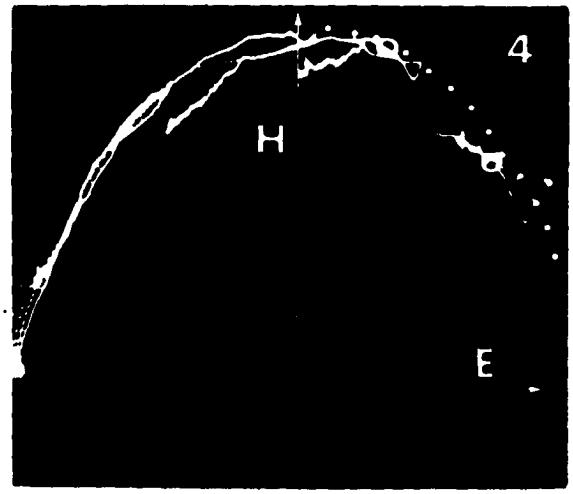
4
H
E

of collapsing decreased with increasing dispersion. This is the added evidence needed to show drastic changes in the magnetization occurred very rapidly.

Assuming a strip model for the magnetization (See Fig. 48) and using the fact that during this process M_L was approximately constant and M_T was not, the following is true:

1. The strips are roughly parallel to the easy axis.
2. The strips are not, in general, of equal width.

With the short duration pulse field, the magnetization never continued rotating, even if it was at an angle greater than 90° with respect to the easy axis.

The following development was to obtain the approximate density or spacing between the walls that were formed within ∿10 nsec after collapsing. For the situation where the film was completely demagnetized, $M_L = 0$, the strips would be approximately of equal width and parallel to the easy axis. Since $H_T \geq .25\ H_K$ was on during the longitudinal pulse interruption, Ne'el type of walls should form. (23) Using Middelhoek's angular dependance for wall energy (23), the energy density /unit thickness/unit wall length becomes equal to

$$E = \frac{1}{2}[b(E_1 + E_2) + \gamma_{N_{1,2}} + \gamma_{N_{2,1}}] \qquad (4a)$$

where E_i - energy/unit vol. of strip i (i = 1,2)

$\gamma_{N_{i,j}}$ - Ne'el wall energy per unit area between strips i and j ($i \neq j$; i,j = 1,2)

b - width of the strips

With $H_{K_1} = H_{K_2}$ (Fig. 48), $\phi_2 = \pi - \phi_1$,

this means

$$E_1 = E_2 \text{ and } \gamma_{N_{1,2}} = \gamma_{N_{2,1}} .$$

Hence,

$$E = b[-M H_T \sin\phi + \frac{M H_K}{2} \sin^2\phi] + \gamma_N(180°)[1-\sin\phi]^2 \qquad (4b)$$

ϕ - angle between the magnetization in one of the strips and the easy axis

H_T - steady applied field in the hard direction

$\gamma_N(180°)$ - energy density of a 180° Ne'el wall.

Minimizing equation 4b with respect to ϕ and using the fact that the collapsed value of M_T is

$$M_T = M \sin\phi \qquad (5)$$

the expression for b was

$$b = \frac{2\,\gamma_N(180°)}{M} \left(\frac{M-M_T}{M_T H_K - M H_T}\right) \qquad (6)$$

By substituting in the value of M_T after collapsing and the transverse field, H_T, and using $\gamma_N(180°) = 8\ 10^{-3}$ joules/m^2, equation 6 calculated strip width from 100 μm for film 1 to 10 μm for film 4. It must be emphasized that this is a very crude calculation, but it does give an idea of the dimensions involved.

The collapsed state was observed using films 1 and 4 with bitter patterns. A steady transverse field of .5 H_K was on during both switching and observing. Strip domains similar to Methfessel (11) and Stein (14) were found. The wall spacings qualitatively agreed with the electrical

measurements, although no quantitative optical measurements were made. As the longitudinal pulse amplitude was increased keeping H_T constant, the angle the walls made with the positive easy axis direction (Fig. 3) changed from approximately 150° to 180°. In the meantime, more and more of the film area switched, leaving a smaller number of unswitched strips or domains. For some excellent Kerr pictures of interrupted switching see Stein (14).

A number of measurements were made where the longitudinal field started again after the switching had been interrupted. The experimental setup is described on page 10. For film 1, Fig. 38 shows that $\overline{M}$ did not continue switching as before the interruption when the time between pulses was 25 nsec. Fig. 39 shows the longitudinal voltage for film 3 for a number of different field conditions. The idea of this measurement was, in addition to the transverse bias, to apply an aiding steady field parallel to the pulse field. However, the magnitude of the total longitudinal field was kept a constant by reducing the pulse field. It was hoped that the D.C. fields would stabilize the domain configuration and keep them from collapsing when the pulse field stopped. If this occurred, the resulting wave form would look like the uninterrupted one except for being segmented, Fig. 39b (conventional domain configurations are stable for pulse interruption experiments (2, p 540)). The results show that there is no stabilization, but, in fact, just the opposite. Evidently, the walls which form and move during the slow part of the flux reversal have a low coercive force, and once they are formed, a much lower applied field will keep them in motion. This observation is consistant with one of Stein's conclusions--formed walls are very broad and slenderize with time.

Fig. 39. Interrupted longitudinal wave forms, LVW, for film 3
$H_T = .2\ H_K$, $H_L = 1.1\ H_K$

a. Uninterrupted wave form

b. Interrupted wave form <u>if</u> the walls stabilized

c. Interrupted wave form where $H_{L_{pulse}} = 1.1\ H_K$, $H_{L_{steady}} = 0\ H_K$

d. Interrupted wave form where $H_{L_{pulse}} = .9\ H_K$, $H_{L_{steady}} = .2\ H_K$

e. Interrupted wave form where $H_{L_{pulse}} = .7\ H_K$, $H_{L_{steady}} = .4\ H_K$

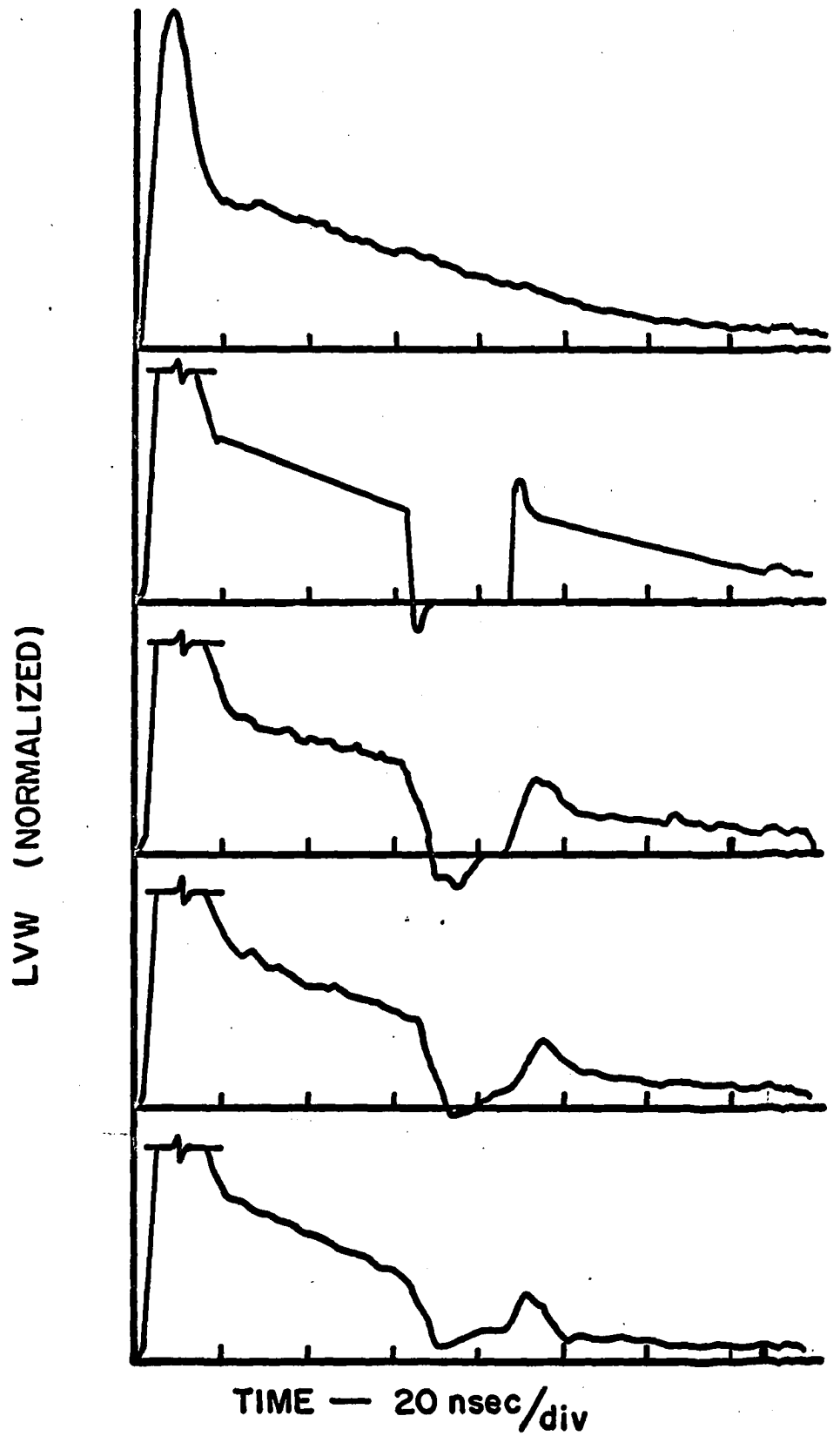
LVW (NORMALIZED)
TIME — 20 nsec/div

However, it was found that the shorter the time interval between the pulses, the more the second wave form looked like the continuation of the first. With a 1.5 msec. delay, the resulting wave form bore no resemblance to the initial one.

IV. THEORETICAL RESULTS

A. Introduction

A number of models have been proposed to describe thin magnetic film switching. The most prominent are the rotation, spin-wave, and strip domain models. The purpose of Chapter 4 is to determine the characteristic of each model and compare them with experiment. Quantitative theoretical results consist of computing with a digital computer the longitudinal and transverse voltage wave forms and in some instances the trajectoires of the net magnetization. To better compare these ideal voltages to those observed experimentally, the theoretical voltages were modified by taking into account the finite band pass characteristics of the sensing system.

It was found that none of the three models adequately described the physical phenomenon. However, the strip domain is found to be the best qualitatively.

B. Filter

To compare theory with practice, it was necessary to know how the sensing system distorted the ideal voltages of the various models. In other words, if the predicted voltages did exist, what would they look like when detected with the experimental apparatus. Since this was a linear filter problem, Laplace transforms (19, p 100) were used. Then

$$V_f(s) = G(s)\, V_i(s) \tag{7}$$

$V_f(s)$---filtered ideal voltage

$G(s)$ ---transfer function of the sense system

$V_i(s)$---ideal voltage predicted by a model

s ---denotes that the Laplace transform has been made

Using the convolution integral, the solution to equation 7 is

$$V_f(t) = \int_0^t V_i(T)\, G\,(t-T)\, dT \qquad (8)$$

where $V_f(t)$, $V_i(t)$, $G(t)$ are the inverse Laplace transforms of $V_f(s)$, $V_i(s)$, $G(s)$. (19, p 85)

The G(s) was determined by means of the following argument. If $V_i(t)$ is a delta function, $\delta(t)$, then by its sifting property, equation 8 becomes

$$V_f(t) = G(t) \quad . \qquad (9)$$

Experimentally, a $\delta(t)$ was supplied to the sense system and the resulting measured wave form was then G(t), Fig. 40. For experimental details see page 20. The G(t) was very similar to a nonoscillatory, 3rd order system, which was consistent with treating the sense coil as an inductor and the oscilloscope as a R.L.C network. (19, p 131)

To find any $V_f(t)$ digitally, the following approximation was made

$$V_f(t) = \Delta t \sum_I V_i(I)\, G(t-1) \qquad (10)$$

where $I = 0, \Delta t, 2\,\Delta t, \ldots, t$.

The transfer function G(t) is normalized so that

$$\int_0^\infty G(t)\, dt = 1 \qquad (11)$$

Equation 11 says that there is no net attenuation or amplification in the filtering, only distortion due to finite rise time. If, then, V_i is a low enough frequency signal,

$$V_f = V_i \; . \qquad (12)$$

Fig. 40. Measured impulse response of the sensing system

Fig. 41. Example of a filtered and unfiltered longitudinal voltage wave form predicted by the rotation model using film 1 parameters, $H_T = .1\ H_K$, $H_L = 1.0\ H_K$

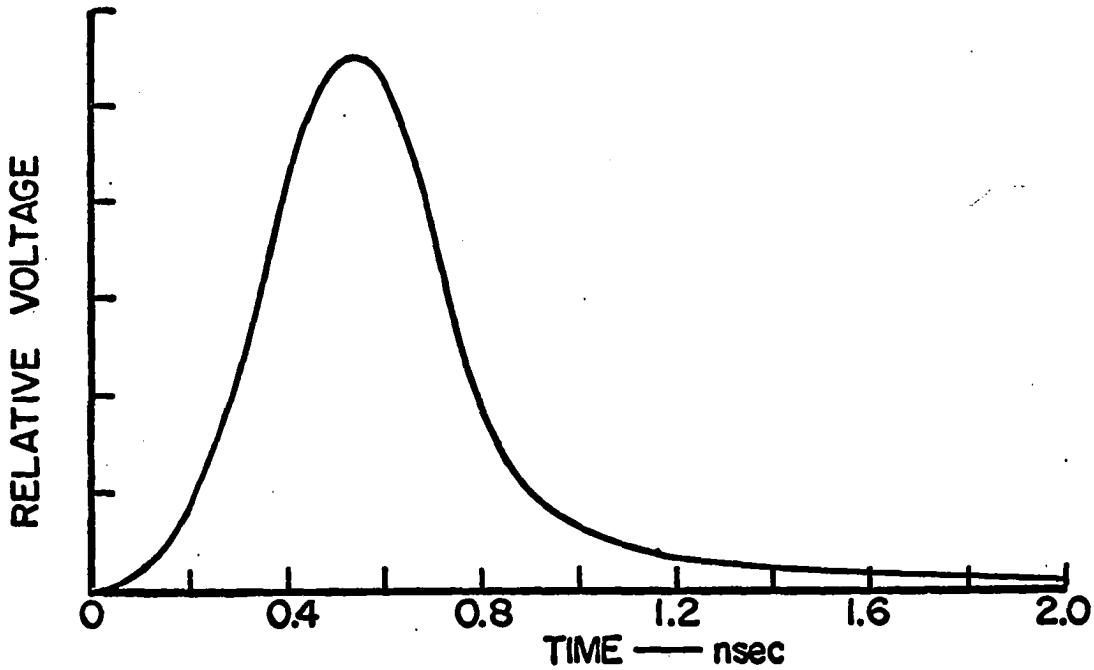
RELATIVE VOLTAGE
0
0.4
0.8
1.2
1.6
2.0
TIME — nsec

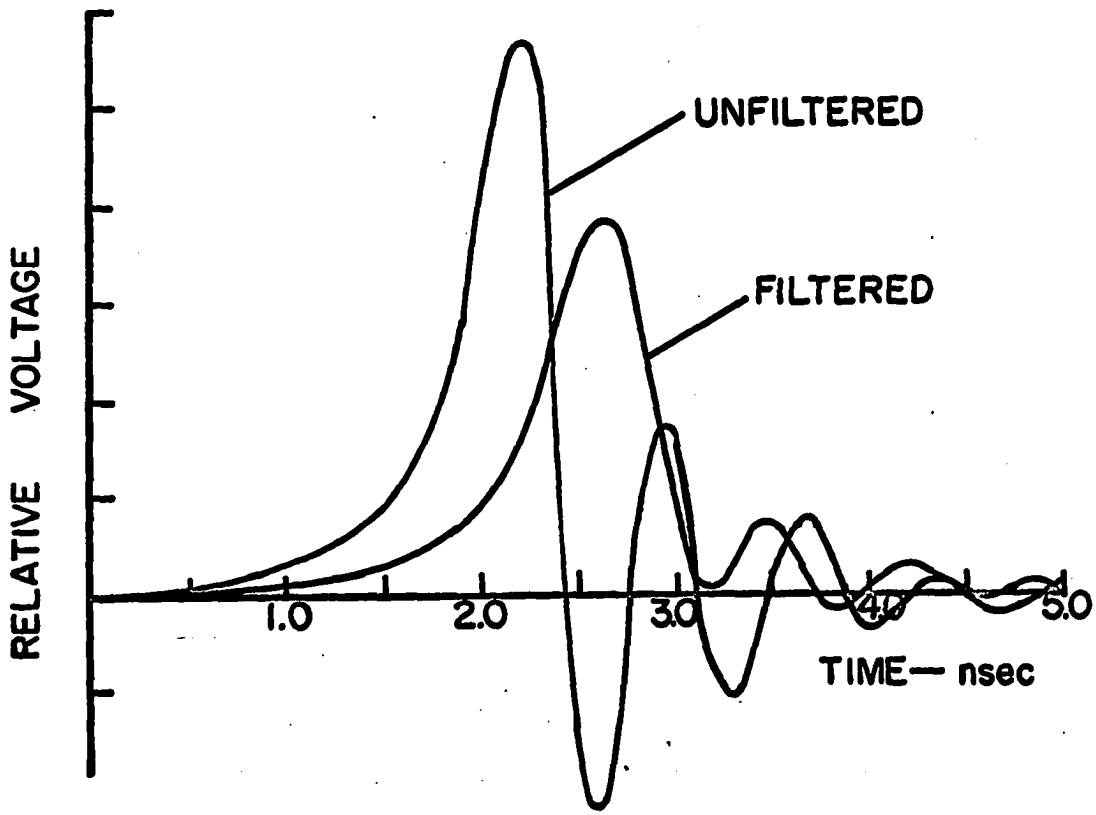
RELATIVE VOLTAGE
UNFILTERED
FILTERED
1.0
2.0
3.0
4.0
5.0
TIME— nsec

For more discussion of this technique see Nilsson and Brown. (19, p 115)

An example using the pure rotation model with $\alpha = .008$, $H_T = .1\ H_K$, and $H_L = 1\ H_K$ is shown in Fig. 41. Note how the drastic oscillations have been reduced by filtering. Some people have tried to infer damping constants from switching times without taking into account equipment rise times. (8) By solving the rotation model for various α's, it was found that the α obtained by τ_s measurement from filtered wave forms could be easily twice the intrinsic value. Therefore, the anomalously high values of α reported in the literature for large angle switching can be attributed in part to instrument response time.

C. Rotation Model

For this model one assumes the perfect situation where the magnetization and the anisotropy are uniform. However, when a field is applied to a magnetic sample, the net magnetization does not precess about the field forever but reaches an equilibrium position. The loss of energy is included in the gyromagnetic equation by introducing a phenomenological damping term. Gilbert introduced this term, as did Landau and Lifshitz. For small losses as in the case of thin films, the two equations of motion are equivalent.

The reversal for pure rotation is a two step process:

1. Upon applying a field in the plane of the film, the magnetization initially rotates at right angles to the field since the torque = $\overline{M} \times \overline{H}$.
2. As $\overline{M}$ rises out of the plane, a very large demagnetization field ($\sim$100 oe) builds up in the film perpendicular to the surface.

This field dominates, and $\overline{M}$ now processes about it until reaching an equilibrium position.

The filtered longitudinal voltages, using Gilbert's equations of motion, equations 41 and 42, were found. The solutions with film 1 parameters are illustrated in Fig. 42 and film 4 parameters in Fig. 43. These are to be compared with the experimental voltages in Figs. 15 and 16. Obviously, when the dispersion of a film became large, as with film 4, there was vertually no correlation between the theoretical and experimental results. However, for low dispersions there was a good correlation with large transverse biases. When this field was reduced, discrepancies appeared. An experimentally observed rule of thumb is that if the magnetization's initial angle, $\phi(0)$, is greater than 3 times the angular dispersion, the behavior of the film is described fairly well by Gilbert's model.

D. Spin-Wave Model

Observing the magnetization in detail, it is found <u>not</u> to be uniform, Fig. 2. This is due to nonuniformities of the induced anisotropy, crystalline anisotropy of the individual crystallites, magnetostriction between crystallites and any other inhomogenity. These stray energies give rise to an effective field, which is a function of position in the film, causing "ripple". The spin-wave model attempts to find the effect the ripple has on magnetization reversal. The easiest way to see how an interaction arises is to express $\overline{H}_{eff}$ as a Fourier series

$$\overline{H}_{eff}(\overline{r},t) = \sum_{\underline{k}} \overline{H}_{\underline{k}}(t)\, e^{i\,\overline{k}\cdot\overline{r}} \qquad (13)$$

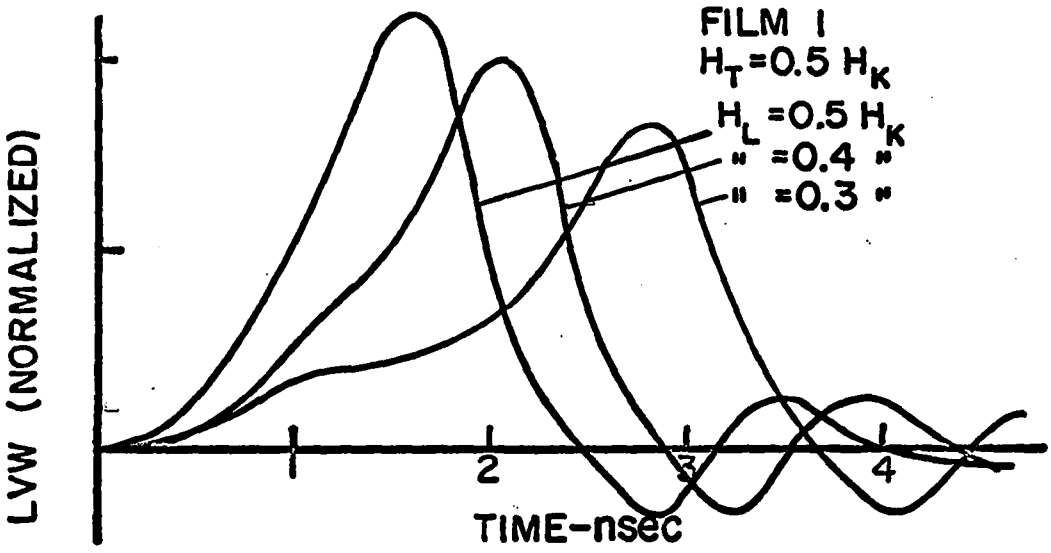

Fig. 42. Longitudinal voltage wave forms using Gilbert's equations of motion and film 1 parameters

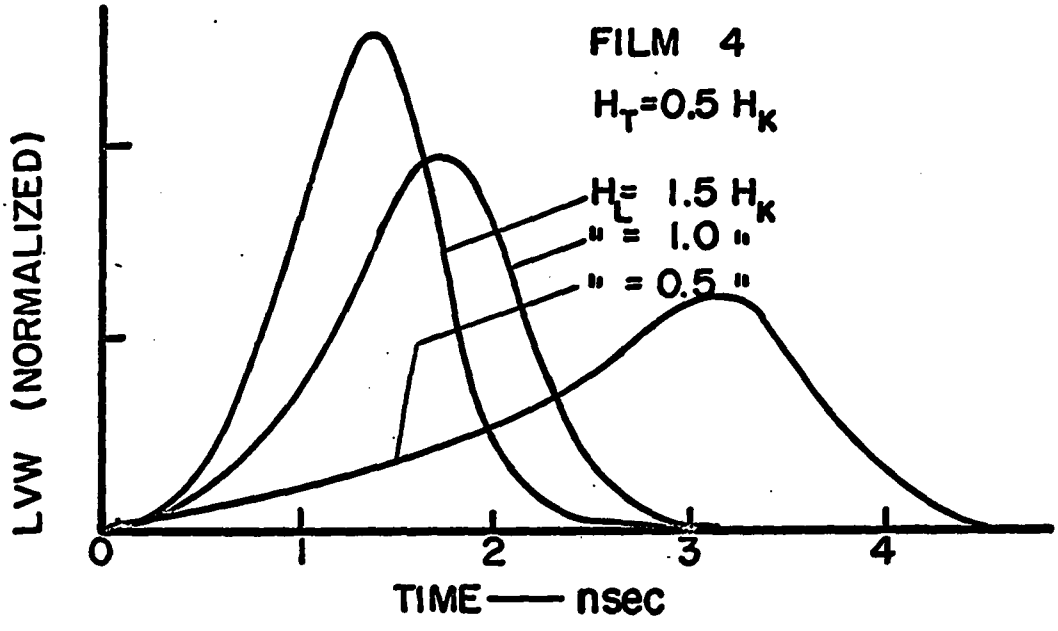

Fig. 43. Filtered longitudinal voltage wave forms using Gilbert's equations of motion and film 4 parameters

$\bar{k}$ ---wave number

$\bar{H}_k$---Fourier coefficient of the effective field

$\bar{r}$ ---position vector

Since $\bar{H}_{eff}$ is a function of distance, $\bar{M}$ will also vary in the plane of the film, so

$$\bar{M}(\bar{r},t) = \sum_{\bar{k}} \bar{M}_k (t)\, e^{i\, \bar{k}\cdot\bar{r}} \tag{14}$$

$\bar{M}_k$---Fourier component of the magnetization

When these two expressions are then substituted into the gyromagnetic equation, page 88, the equation of motion for $\bar{M}_o$ (the net magnetization) is

$$\frac{d\bar{M}_o}{dt} = -\gamma \bar{M}_o \times \bar{H}_o - \gamma \sum_{\bar{k}\neq o} \bar{M}_k \times \bar{H}_{-k} \tag{15}$$

The damping term has been lumped into the $\bar{H}_k$'s. This is exactly the same expression as for the pure rotation model except for the last term on the right hand side, which is the nonlinear reaction of the "spin-waves" on $\bar{M}_o$. What Harte calls "spin-waves" are just the Fourier coefficients, $\bar{M}_k$, or the classical continuum picture of spin-waves.

Harte's contribution was to solve the equations of motion of $\bar{M}_k$ and then put the solutions back into equation 15. Since the solution $\bar{M}_k$ was an initial value problem, the distribution of $\bar{M}_k$ at time t = 0 had to be found. A statistical model was used where the uniaxial strain-induced anisotropy was assumed to vary randomly in direction from crystallite to crystallite.

A number of approximations had to be made to obtain a solution. The

most basic one (in the opinion of the author) was that $\overline{M}_o(t)$ rotates faster than the initial spin-waves can either, 1) relax to a new position or 2) become unstable. More will be said about this assumption later.

The magnetization is found to go through a transient state of high magnetostatic energy (see Appendix D) and a spin-wave reaction torque is exerted on the uniform mode, $\overline{M}_o(t)$. This torque, which is proportional to the square of the angular dispersion, opposes rotation up to 90° from $\overline{M}_o$'s initial angle, then aids it. In other words the spin-waves absorb energy for the first 90°. Since the waves do not relax, they transfer the energy back to the uniform mode during the last part of the reversal.

If the applied field is not large enough to overcome this reaction torque, the magnetization is locked and can not proceed by rotation. Harte then speculated that reversal would continue at a much slower rate determined by the spin-waves' relaxation rate.

In summary this spin-wave model predicts:

1. An overall slower switching time due to the reaction torque retardation during the 1st quadrant of rotational switching.
2. Locking of the uniform mode for fields greater than those predicted by Stoner-Wohlfarth, (i.e. larger fields are needed to have rotational switching).
3. The effects of angular dispersion on 1 and 2.

The crucial test for the proposed theory is to solve the equations of motion with experimentally determined parameters and to compare the resulting voltages with the observed ones. The reaction torque parameter was obtained by plotting on the Stoner-Wohlfarth asteroid the fields needed to switch 50% of the magnetization by fast rotation for the various films,

Fig. 28. These fields were compared with the predicted curves with their corresponding reaction torque coefficient, R. (See Appendix C and Harte, 6) The necessity for choosing the 50% criterion was due to the fact that there was no sharp threshold for rotational switching. The results are shown in Figs. 44 and 45 and should be compared with Figs. 15 and 16.

The agreement is not good, especially for low fields. The problem was the cosine angular dependence in the reaction torque term (equation 48). This means the retardation was a maximum before the net magnetization began to rotate. Experimentally, this was not the case as shown by the rapid build up of the LVW.

A mathematical difficulty introduced this cosine term. Since the WKB method was used to find $\overline{M}_{\overline{k}}$ for $\overline{k} \neq 0$, the solution became unbounded at the free points which are at $\phi(o)$ and $\phi(o) + \pi$ (See Fig. 3). However, when this singular solution was substituted into the expression for the reaction torque term, a multiplying factor

$$\frac{\sin 2\,(\phi(t) - \phi(o))}{\sin\,(\phi(t) - \phi(o))} \tag{16}$$

was obtained. The numberator is a result of the magnetostatic interaction as demonstrated in equation 64, and the denominator is the singularity introduced by the WKB solution. By using trigonometry identities, $2 \cos\,(\phi(t) - \phi(o))$ was the final angular dependence. Harte mentions this difficulty and states that his equations of motion hold after a "short build up time", thus making the strict application of his model very awkward.

A number of solutions using Harte's equations were made, but with $\sin 2\,(\phi(t) - \phi(o))$ replacing the cosine form, Figs. 46 and 47. The

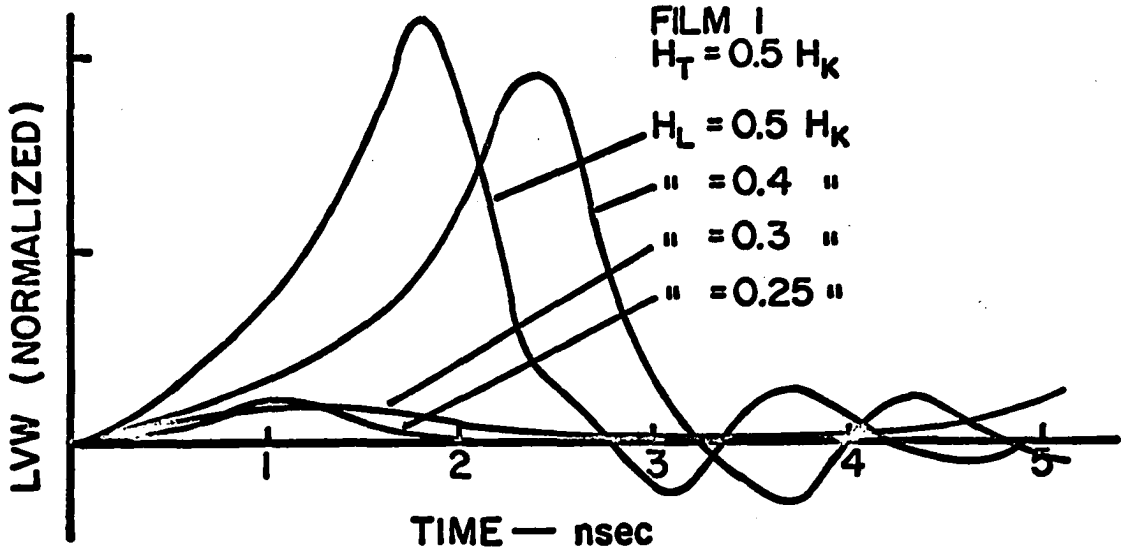

Fig. 44. Filtered longitudinal voltage wave forms using Harte's equations of motion and film 1 parameters

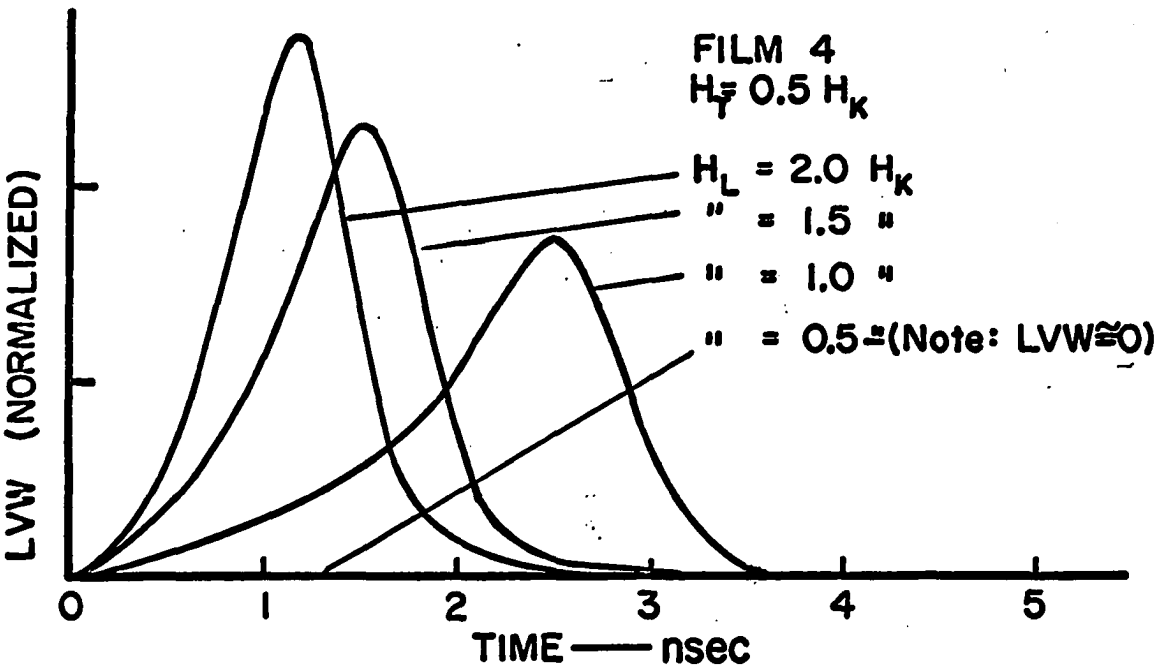

Fig. 45. Filtered longitudinal voltage wave forms using Harte's equations of motion and film 4 parameters

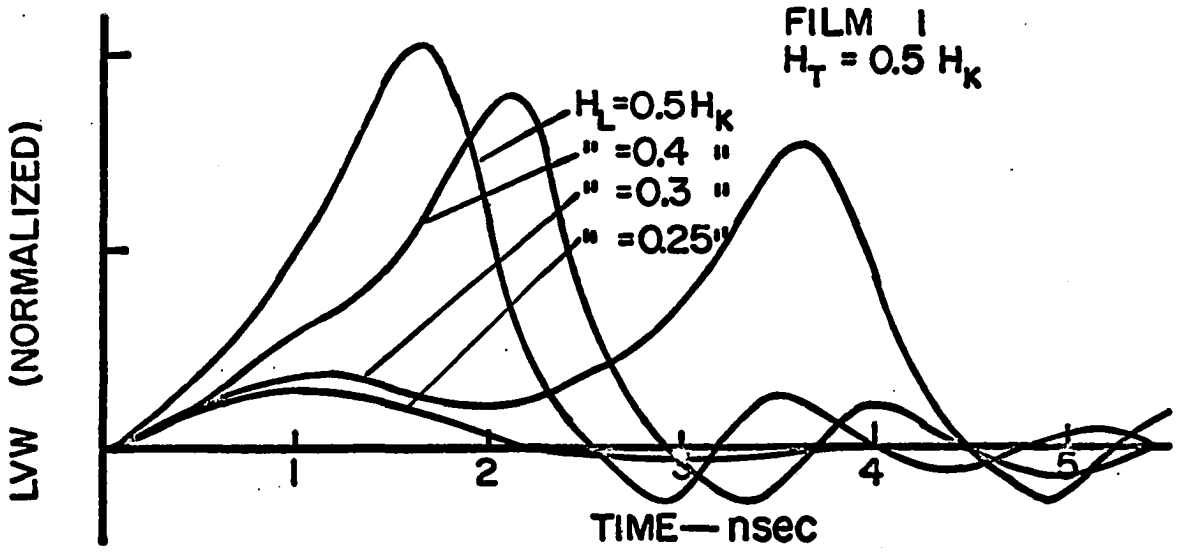

Fig. 46. Filtered longitudinal voltage wave forms using modified Harte's equations and film 1

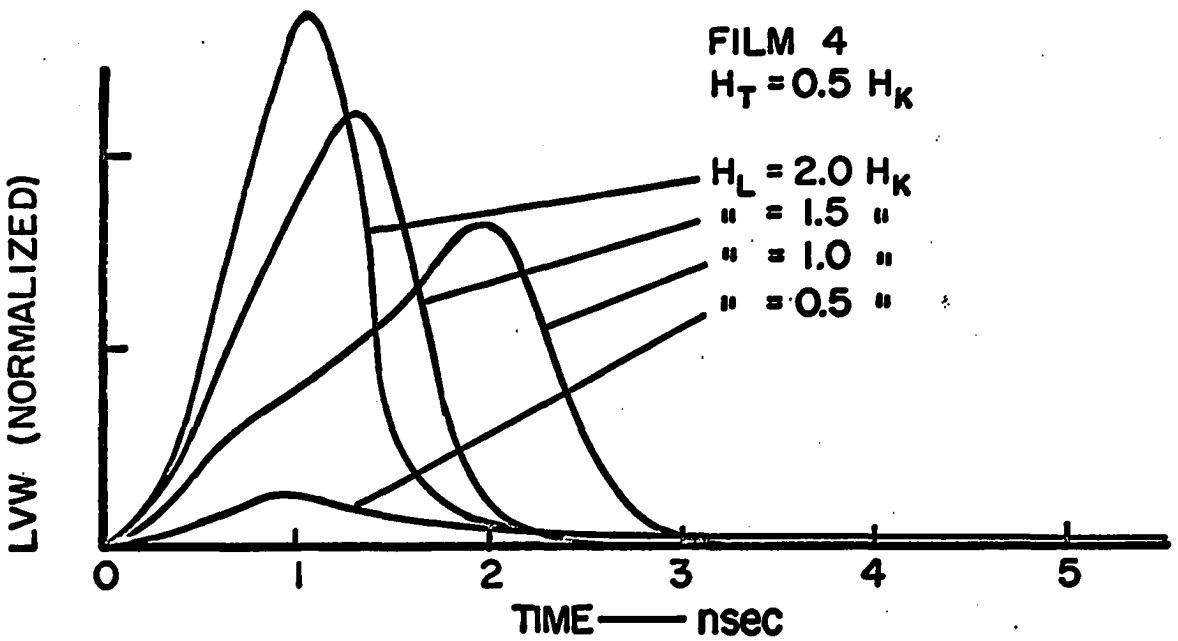

Fig. 47. Filtered longitudinal voltage wave forms using modified Harte's equations and film 4

agreement is better than before, especially for low dispersion films. However, there are still some shortcomings.

Neither the cosine or sine versions have the ability to:

1. Predict all observed wave forms.
2. Have locking occur for all angles as seen by the trajectory measurements.
3. Account for the irreversible behavior for applied pulses shorter than the switching times.

Also, aiding, page 73, is never seen for $\phi(t) \geq \phi(o) + \frac{\pi}{2}$.

In the author's opinion the main trouble with Harte's theory is that instabilities and rapid rearrangements of the spin-waves occur during reversal. Hence, the basic assumption that the net magnetization can rotate faster than build-ups or relaxations of the ripple is incorrect.

E. Strip Domain Model

The calculations in this section attempt to show that instabilities of the magnetization can cause locking. The model used was highly simplified and relied on the static observation the well defined strips perpendicular to the net magnetization appear if fields slowly (in terms of seconds) approach the rotational threshold. (11) Once formed, the strips prevent rotation so that higher applied fields must be used to complete the switching by either wall motion or rotation. The explanation for this behavior was that the ripple due to variations in the film parameters became unstable. For more information see Smith and Harte (8) or Methfessel et al. (11)

Thomas proposed a model for these observations by assuming the film

consisted of parallel strips, Fig. 48. Alternate strips having different anisotropy constants, H_K, were coupled magnetostatically by the resulting free magnetic pole which arose when the normal component of the magnetization was not constant across an interface.

To use this model for fast switching further assumptions and restrictions were made. One was that Gilbert's model holds true for each strip with the coupling fields included. The other was that the strips moved with the net magnetization until they became unstable at an angle ϕ_i. The magnetization reversal for this model can be explained as follows:

1. At time t = 0, with the strips perpendicular to the net magnetization, $\langle\bar{M}\rangle$, the angles ϕ_1 and ϕ_2 were determined by the steady applied field, H_T, and the respective H_K values. Equation 36b simplifies to
$$\phi_j(o) = \sin^{-1} H_T/H_{K_j} \quad (j = 1,2) \tag{17}$$
2. After the pulse field, H_L, was turned on, the strips remained perpendicular to the rotating $\langle\bar{M}\rangle$.
3. When <M> reached an angle ϕ_i, the strips became stationary, simulating an instability. Further rotation gave rise to large internal magnetostatic fields for $\nabla\cdot\bar{M} \neq 0$. If these fields were large enough, switching was inhibited and $\langle\bar{M}\rangle$ was said to be locked.

It was then theorized that the subsequent reversal occurred by the motion of the walls that had been formed by the instabilities. Since the wall motion process was much slower, it could account for the long tail observed on the switching wave forms, Fig. 39.

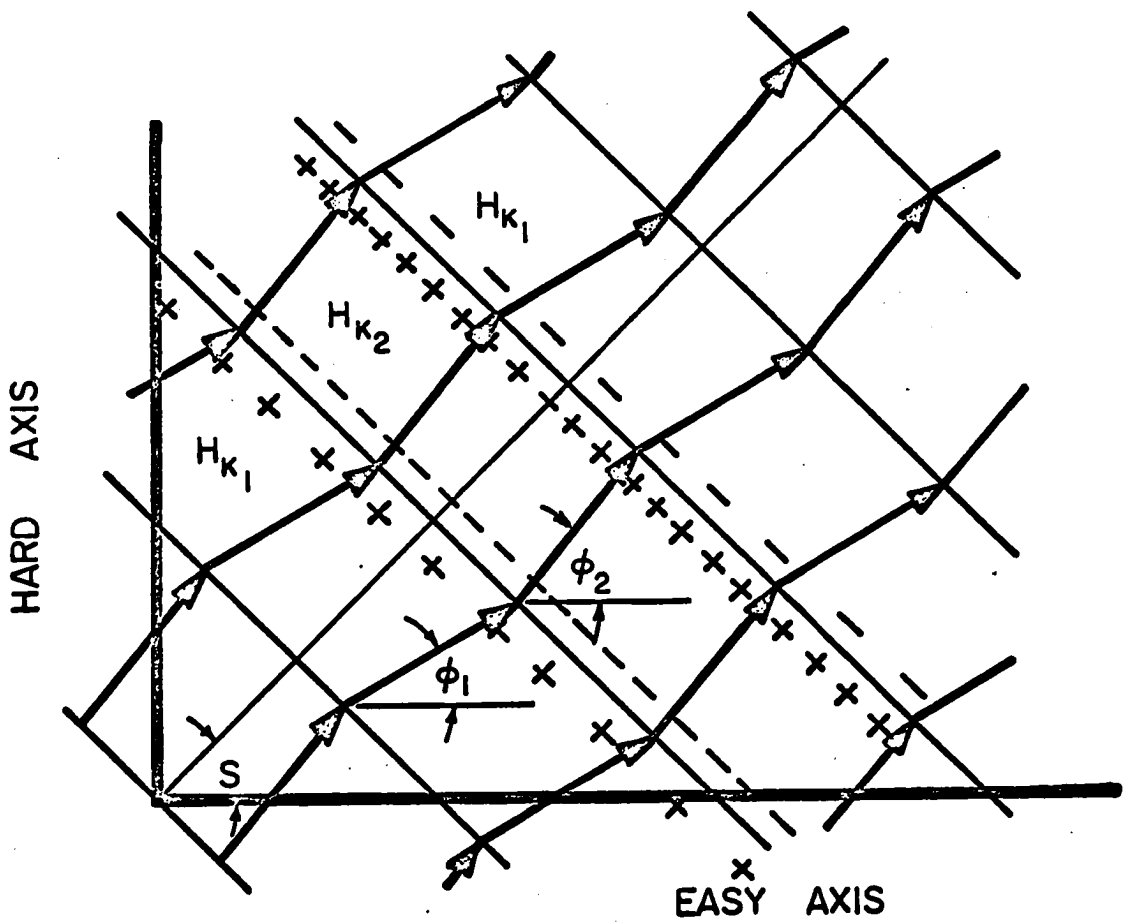

Fig. 48. Strip domain model for thin magnetic film

The constants needed for the equations in Appendix D were found both experimentally and theoretically. First ϕ_i will be discussed.

According to the Stoner-Wohlfarth static theory, the magnetization rotates away from the easy axis as the applied switching field is slowly increased. When $\phi_{critical}$ is reached, irreversible rotation occurs. The expression for this angle is (page 92)

$$\phi_{critical} = \sin^{-1} (H_H/\langle H_K \rangle)^{1/3} \qquad (18)$$

H_H = hard axis applied field

$\langle H_K \rangle$ = average anisotropy field

With fields close to the rotation threshold, $\phi_{critical}$ was used as the angle at which instabilities occurred. Here the uniform rotational torque was approximately zero. Hence, any spurious torques from dispersion, etc., would try to switch various film areas giving rise to instabilities. The interrupted switching measurements to determine irreversibility (page 54) substantiated this angle criterion.

Since Torok's technique is an indication of H_K's amplitude dispersion the resulting distribution curve was symmetrically superimposed about the average H_K. The $\langle H_K \rangle$ value was determined by a hysteresis-looper and checked with a torque magnetometer. The two values where the distribution fell to 50% of its maximum height were chosen for the computer solutions. This is by no means rigerous but adequate for these results.

The wall spacing was derived experimentally as discussed on page 60. These values assume that the strips all had equal width, d, where d>>t, the thickness of the film. Consequently, the angle at which locking occurred for the net magnetization equaled $\phi_{critical}$. However, the locking

angle could be varied in several ways. One was to change the angle where instabilities occur, though this would be contrary to previous qualitative arguments. Another was to make the strips of unequal width while keeping the instability angle equal to $\phi_{critical}$. The latter would correspond to either the way the walls were formed or motion of the walls during their creation. By unequal wall widths $\phi_{locking}$ could be made to occur for practically any experimentally observed angle.

Qualitatively, the results shown in Figs. 49 and 50 are fair; both notches and locking occurred. However, there were discrepancies. First of all, rapid oscillations after locking were not observed, Figs. 14 and 22. Also, the shape of the wave forms differed from experiments.

These shortcomings were caused by extreme simplicity and severity of the model. It did not allow for wall rearrangements or for gradual transition from an unlocked to locked state. The dissipative energy loss was neglected in forming the walls. This could account for the experimentally observed highly damped wave forms upon locking, Fig. 22.

In conclusion, the strip model qualitatively seems to explain all aspects of nonuniform rotation, but falls down quantitatively because of the simplifying assumptions which were made.

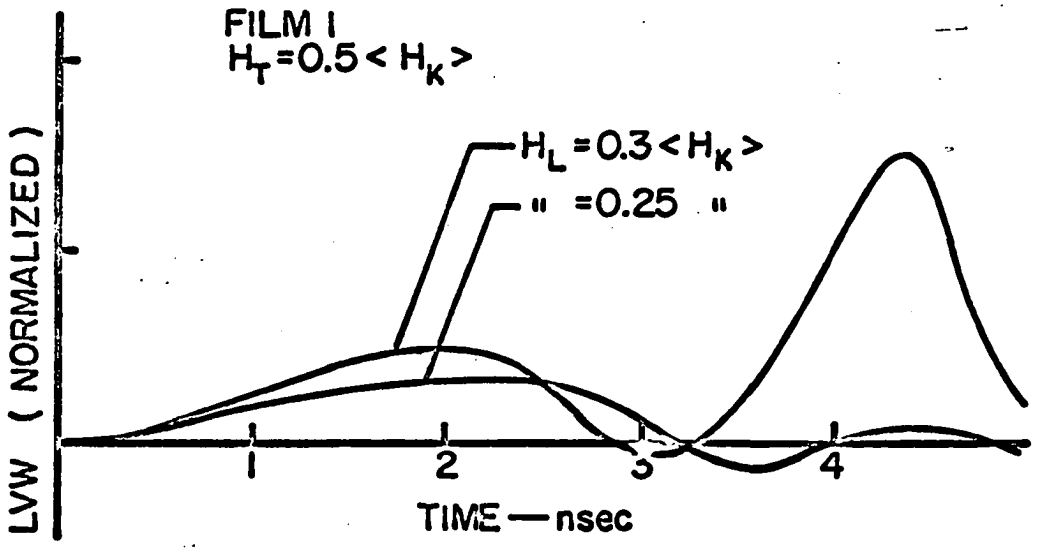

Fig. 49. Filtered longitudinal voltage wave forms using strip domain model and film 1 parameters, b = 100 μm, H_{K_1} = 1.1 H_K, H_{K_2} = .9 H_K

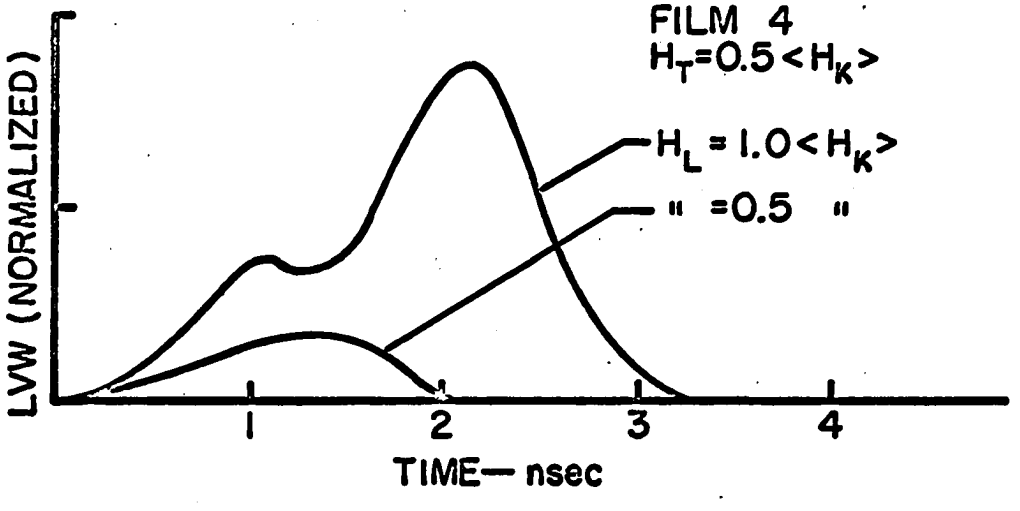

Fig. 50. Filtered longitudinal voltage wave forms using strip domain model and film 4 parameters, b = 10 μm, H_{K_1} = 1.2 H_K, H_{K_2} = .8 H_K

V. CONCLUSIONS

The experimental data of this thesis show that instabilities of the magnetization can occur during flux reversal. The direct consequence is that the net magnetization can lock at all angles with respect to the easy axis. During reversal, instabilities start to grow when the uniform, torque amplitude equals the spurious torques. These torques from the thin film nonhomogenities then tried to cause portions of magnetization to switch. Competition between regions trying to switch and those trying not to switch appears to be the mechanism causing instabilities. The resulting walls that are created were found to be very mobile. Unlike conventional Ne'el or Block walls, they could not be stabilized.

Further investigation with pulse fields shorter than the film's switching time showed that drastic rearrangements of the magnetization can take place in a few nanoseconds. The amount the magnetization collapsed was inversely related to the angular dispersion and was believed to give a measure of the "spacing of the walls" or wave length of the ripple that became unstable. Dispersion can be thought of as a measure of the coupling between film regions; as the dispersion increases so does the coupling.

The experimental data and its interpretation are in direct conflict with Harte's assumption that the magnetization rotates faster than the spin-waves--or ripple pattern--can relax. The data do support a strip domain model. However, with the model chosen for these calculations the quantitative agreement was not good. Also, it was too phenomenological. The ideal theory would be one that starts as Harte's did by developing

equations for ripple amplitudes and wave lengths, but ends up taking into account instabilities.

In summary, noncoherent rotation can be characterized by 1) the magnetization initially rotating uniformly until the dispersion torques overshadow the uniform applied field torques, 2) these spurious torques causing instabilities and forming walls which segment the film 3) the completion of the magnetization reversal with the motion of these walls.

VI. LITERATURE CITED

1. Blois, M. S., Jr. Preparation of thin magnetic films and their properties. J. Appl. Phys. 26: 975-980. 1955.

2. Gyorgy, E. M. Magnetization reversal in nonmetallic ferromagnets. In Rado, G. T. and Suhl, H. eds. pp. 525-551. New York, N.Y., Academic Press Inc. 1963.

3. Pohm, A. V. Magnetic films. In Prywes, N. S. ed. Amplifier and memory devices. pp. 215-298. New York, N.Y., McGraw-Hill Book Co., Inc. 1965.

4. Olson, C. D. and Pohm, A. V. Flux reversal in thin films of 82% Ni, 18% Fe. J. Appl. Phys. 29: 274-282. 1958.

5. Soohoo, R. F. Magnetic thin films. New York, N.Y., Harper and Row. 1965.

6. Harte, K. J. Spin-wave effects in magnetic-film switching. J. Appl. Phys. 35: 960-961. 1965.

7. Wolf, P. Free Oscillations of the Magnetization in Permalloy Films. J. Appl. Phys. 32: 95S-96S. 1961.

8. Smith, D. O. and Harte, K. J. Noncoherent switching in permalloy films. J. Appl. Phys. 33: 1399-1413. 1962.

9. Cohen, M. S. Magnetic measurements with Lorentz microscopy. IEEE Transactions on Magnetics, Mag-k: 156-157. 1965.

10. Harte, K. J. Flux reversal by noncoherent rotation in magnetic films. J. Appl. Phys. 31: 283S-284S. 1960.

11. Methfessel, S., Middelhoek, S. and Thomas, H. Partial rotation in permalloy films. J. Appl. Phys. 32: 1959-1963. 1961.

12. Stoner, E. C. and Wohlfarth, E. P. A mechanism of magnetic hysteresis in heterogeneous alloys. Phil. Trans. Roy. Soc. (London) A240: 599-642. 1948.

13. Thomas, H. A theoretical model for partial rotation. J. Appl. Phys. 33: 1117-1118. 1962.

14. Stein, K. U. Die abhangigkeit der geschwindigkeit der koharenten magnetisierungsdrehung von der dicke und inhomogenitat dunner schichten. Zeitschrift fur angewandte Physik 18: 528-531. 1965.

15. Dietrich, W., Proebster, W. E., Wolf, P. Nanosecond switching in thin magnetic films. IBM J. Research and Develop. 4: 189-196. 1960.

16. Gilbert, T. L. A Lagrangian formulation of the gyromagnetic equation of the magnetic field. (Abstract) Physical Review 117: 1243. 1955.

17. Sie, C. H. Dynamic pulse hysteresis of magnetic devices. J. Appl. Phys. 36: 1066-1067. 1965.

18. Dietrich, W. and Proebster, W. E. Millimicrosecond magnetization reversal in thin magnetic films. IBM J. Research and Develop. 3: 375-376. 1959.

19. Brown, R. G. and Nilsson, J. W. Introduction to Linear Systems Analysis. New York, N.Y., John Wiley and Son, Inc. c1962.

20. Torok, E. J., White, R. A., Hunt, A. J. and Oredson, H. N. Measurement of the easy-axis and H_K probability density function for thin ferromagnetic films using the longitudinal permeability hysteresis loop. J. Appl. Phys. 33: 3037-3041. 1962.

21. Nelson, R. H. Ferromagnetic resonance linewidth and internal biasing field in Ni-Fe films as a function of dispersion in the anisotropy field magnitude. J. Appl. Phys. 35: 808-809. 1964.

22. Bonyhard, P. I. and Buckinghams, I. C. Switching processes in thin ferromagnetic film memory elements. International Conf. Magnetics Proc. 1965: 5.6-1 - 5.6-6. 1965.

23. Middelhoek, S. Domain walls in thin Ni-Fe films. J. Appl. Phys. 34: 1054-1059. 1963.

24. Lax, B. and Button, K. J. Microwave ferrites and ferrimagnetics. New York, N.Y., McGraw-Hill Book Co. 1962.

VII. ACKNOWLEDGMENTS

My sincere gratitude goes to Dr. A. V. Pohm for his guidance and help. Working with him these past four years has been a very rewarding experience. Financial assistance was obtained from the Department of Health, Education, and Welfare; Industrial Affiliate Program in Solid State Electronics at Iowa State University; and a National Science Foundation Grant. Needless to say their help was most appreciated. Special thanks go to Mr. R. A. Sharpe and Mrs. J. F. Smith for the computer programming assistance, Cyclone Computer Laboratory for the use of its computer and facilities, and to Mrs. N. T. Skola for the hours of typing.

VIII. APPENDIX A

General Equations of Motion

An excellent reference for the following developments is by Harte (6) and will be used extensively in this Appendix.

The basic semi-classical equations of motion for the magnetization of a material is

$$\frac{\partial}{\partial t}\bar{M}(\bar{r},t) = -\gamma\,\bar{M} \times \bar{H}_{eff} + \text{damping term} \tag{19}$$

where γ = absolute value of the gyromagnetic ratio

$\bar{H}_{eff}$ = the effective magnetic fields acting on the magnetization (exchange, applied fields, anisotropy fields, internal fields due to the geometry of the thin film and the configuration of the magnetization,...)

This effective field is usually obtained by calculating the free energy, E, because

$$\text{Torque} = \bar{M} \times \bar{H}_{eff} \tag{20}$$

but
$$= \bar{r} \times \bar{F} \tag{21}$$

where $\bar{r}$---unit vector of the magnetization

$\bar{F}$---generalized force

but
$$\bar{F} = -\frac{1}{M}\nabla(E) \tag{22}$$

therefore

$$\bar{H}_{eff} = -\frac{1}{M}\nabla(E) \tag{23}$$

The energy of the induced anisotropy is described phenomenologically by

$$E_a = +\frac{1}{2} H_K M \sin^2\xi \tag{24}$$

H_K---phenomenological anisotropy field

ξ ---angle between $\overline{M}$ and the easy axis

The $\frac{1}{2}$ multiplier is due to the fact that E_a is a self energy.

The internal fields are found from Maxwell's equations

$$\nabla\cdot(\mu_o \overline{H}_{int} + \overline{M}) = 0 \tag{25}$$

$$\nabla \times \overline{H}_{int} = 0 \tag{26}$$

using boundary conditions appropriate to thin films and the specific model (rotation, spin-wave,...) of interest.

The external fields include both the static and dynamic fields.

$$E_{ext} = - \overline{M}\cdot\overline{H}_{ext} \tag{27}$$

IX. APPENDIX B

Rotation Model

The following assumptions are made:

1. $\overline{M}$ is not a function of position in film and M equals a constant.
2. $\overline{H}_{eff}$ includes only demagnetizing fields, external fields, and the anisotropy field.
3. The damping constant is (16)

$$+ \frac{\alpha}{M} \overline{M} \times \frac{d\overline{M}}{dt} \tag{28}$$

where α is a positive, dimensionless constant.

Using various vector identities, the final vector equation becomes

$$(1+\alpha^2)\frac{d\overline{M}}{dt} = - \gamma \overline{M} \times \overline{H}_{eff} - \frac{\alpha\gamma}{M} \overline{M} \times (\overline{M} \times \overline{H}_{eff}) \tag{29}$$

With the spherical coordinate system as shown in Fig. 51, the spatial components are

$$(1+\alpha^2)\frac{d\theta}{dt} = - \frac{\gamma}{M} \frac{\partial E}{\partial \phi} - \frac{\alpha\gamma}{M} \frac{\partial E}{\partial \theta} \tag{30}$$

$$(1+\alpha^2) \sin\theta \frac{d\phi}{dt} = \frac{\gamma}{M} \frac{\partial E}{\partial \theta} - \frac{\alpha\gamma}{M} \frac{\partial E}{\partial \phi} \tag{31}$$

The demagnetizing fields (or internal fields) of a magnetic sample in the shape of a general ellipsoid are uniform and equal

$$\overline{H}_d = - N \overline{M}/\mu_o \tag{32}$$

where N is a diagonal 3 x 3 matrix called the demagnetizing factor. (24, p 157) For a large circular thin film $N_x = N_y << N_z = 1$. The resulting energy (ignoring the x & y components) is

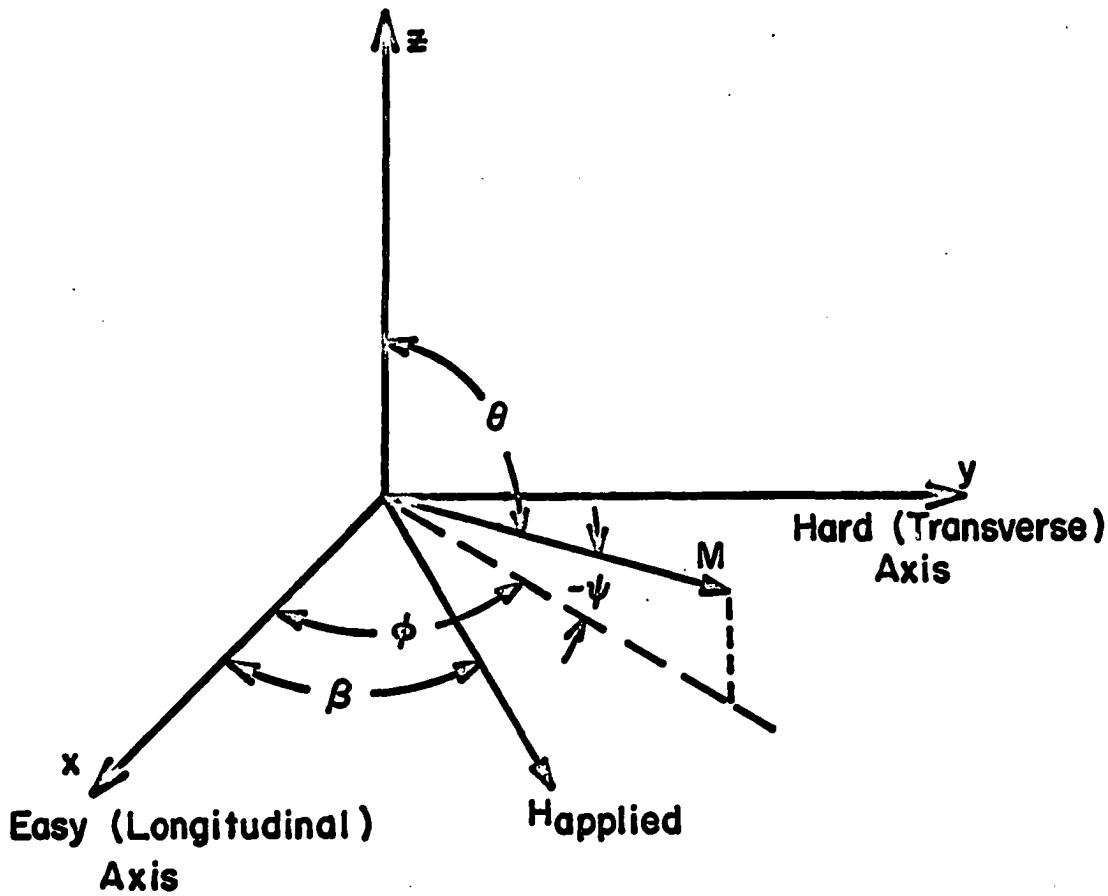

Fig. 51. Coordinate system for thin magnetic film

$$E_d = \frac{1}{2}\frac{M^2}{\mu_o}\cos^2\theta \tag{33}$$

The total energy is

$$E_t = E_a + E_{ext} + E_d \tag{34a}$$

$$= -\frac{1}{2} H_K M \sin^2\theta \cos^2\phi + \frac{1}{2}\frac{M^2}{\mu_o}\cos^2\theta$$

$$- M H \sin\theta \cos(\phi-\beta) \tag{34b}$$

Then

$$\frac{1}{M}\frac{\partial E}{\partial \theta} = - H \cos\theta \cos(\phi-\beta) - \frac{M}{2\mu_o}\sin 2\theta - \frac{1}{2} H_K \sin 2\theta \cos^2\phi \tag{35}$$

$$\frac{1}{M}\frac{\partial E}{\partial \phi} = H \sin\theta \sin(\phi-\beta) + \frac{1}{2} H_K \sin^2\theta \sin 2\phi \tag{36a}$$

For the static situation the above two equations must equal zero. In other words, the energy must be minimized. This occurs for $\theta = \frac{\pi}{2}$, ($\overline{M}$ in the plane of the film). Equation 36a now simplifies to

$$H_L \sin\phi + H_T \cos\phi = H_K \sin\phi \cos\phi \tag{36b}$$

giving the equilibrium position of the magnetization for all applied fields.

To find the critical fields which predict the onset of rotation, the inflection point of E versus ϕ must be calculated.

$$\left.\frac{1}{M}\frac{\partial^2 E}{\partial \phi^2}\right| = H \cos(\phi-\beta) + H_K \cos 2\phi \tag{37}$$

$$\theta = \frac{\pi}{2}$$

Solving 36b and 37 simultaneously after 37 has been set equal to zero, the following two equations are obtained

$$H_L = - H_K \cos^3\phi \tag{38}$$

$$H_T = H_K \sin^3\phi \tag{39}$$

The result, the Stoner-Wohlfarth critical fields for rotation, is shown in Fig. 28. (12)

For applied fields $<<M/\mu_o$, the magnetization stays very nearly in the plane during fast reversal. Letting $\psi = \theta - \frac{\pi}{2}$ where ψ is now small, and making use of the fact that $H_K \sim 300$ amp turns $/m<<M/\mu_o$, 35 and 36a now become

$$H_\theta = -\frac{1}{M}\frac{\partial E}{\partial \theta} \doteq -\frac{M}{\mu_o}\psi \tag{40a}$$

$$H_\phi = -\frac{1}{M}\frac{\partial E}{\partial \phi} \doteq -H\sin(\phi-\beta) - \frac{1}{2}H_K \sin 2\phi \tag{40b}$$

The final equations of motions are

$$\frac{d\phi}{dt} = +\frac{\alpha\gamma}{1+\alpha^2}H_\phi + \frac{\gamma M}{(1+\alpha^2)\mu_o}\psi \tag{41}$$

$$\frac{d\psi}{dt} = +\frac{\gamma}{1+\alpha^2}H_\phi - \frac{\alpha\gamma M}{(1+\alpha^2)\mu_o}\psi \tag{42}$$

The first term on the right hand side of equation 41 is small compared to the second term, thus simplifying the equations even further. Essentially, the disparity means that the rotation in the ϕ direction is due mainly to the Z directed demagnetizing fields.

X. APPENDIX C

Spin-Wave Model

In Fig. 2 the magnetization is not uniform, but rippled. The spin-wave model attempts to determine the effect of the ripple on magnetization reversal. The development of the equations in this Appendix will be very brief, for detailed calculations see Harte (6).

Let

$$\bar{M}(\bar{r},t) = \sum_{k} \bar{M}_k(t) e^{i\,\bar{k}\cdot\bar{r}} \tag{43}$$

$$\bar{H}_{eff}(\bar{r},t) = \sum_{k} \bar{H}_k(t) e^{i\,\bar{k}\cdot\bar{r}} \tag{44}$$

$\bar{k}$ - wave vector

$\bar{r}$ - position vector

Using 19 (Harte neglected damping) the uniform mode equation becomes

$$\frac{d\bar{M}_o}{dt} = -\gamma\,\bar{M}_o \times \bar{H}_o - \gamma \sum_{k\neq o} \bar{M}_k \times \bar{H}_{-k} \tag{45}$$

This second term is a nonlinear reaction torque due to the spin-waves (i.e. the Fourier components of the magnetization). The problem is solved if $\bar{M}_k(t)$ can be evaluated. By assuming $\bar{M}_k(t)$ is only coupled to $\bar{M}_o(t)$, the equation of motion for $\bar{k} \neq 0$ becomes

$$\frac{d\bar{M}_k}{dt} = -\gamma\,(\bar{M}_o \times \bar{H}_k - \bar{H}_o \times \bar{M}_k) \tag{46}$$

The $\bar{H}_k$ includes exchange, magnetostatic contributions due to the ripple, uniaxial anisotropy, and random anisotropies which give rise to the magnetization ripple.

The basic assumption made in Harte's solutions of the $\bar{M}_k$'s is that

the original spin-waves do not die out or become unstable <u>during</u> the magnetization reversal. In other words, $\overline{M}_o(t)$ rotates faster than the spin-waves can relax, and the magnetization goes through a transient state of high magnetostatic energy.

After much labor (86 pages of Ph.D. thesis), Harte found $\overline{M}_k(o)$, $\overline{M}_k(t)$ and $\overline{H}_k(t)$. Substituting these expressions into equation 45 and including damping of the uniform mode, the result is

$$\frac{d\phi}{dt} = + \frac{\gamma M}{(1+\alpha^2)\ \mu_o}\ \psi \tag{47}$$

$$\frac{d\psi}{dt} = + \frac{\gamma}{1+\alpha^2} H_\phi - \frac{\alpha\gamma M}{(1+\alpha^2)\ \mu_o}\ \psi - \gamma\ H_K\ R\ F\ \cos(\phi-\phi(o)) \tag{48}$$

where

$$R = 3.1\ 10^{+3}\ M\left(\frac{t^2}{H_K A}\right)^{1/3}\ \delta^2 \tag{49}$$

$$F = \frac{\{h_p\ \sin[\beta_p - \phi(o)]\}^{1/3}}{\{\cos 2\phi(o) + h_b\ \cos[\beta_b - \phi(o)]\}^{5/12}} \tag{50}$$

where

t - film thickness

A - exchange constant, 10^{-11} joules/m

δ - R.M.S. of angular dispersion, radians

H_K - uniaxial anisotropy

h_p - pulse field magnitude/H_K, dimensionless

h_b - D.C. bias field magnitude/H_K, dimensionless

β_b, β_p - angles between easy axis and bias and pulse fields respectively

XI. APPENDIX D

Strip Domain Model

Large angle calculation

The following characteristics are assumed:

1. The magnetization is not uniform over the plane of the film but consists of parallel strips, Fig. 48, in which magnetization is uniform.
2. Alternating strips or bands have different anisotropy constants H_{K_1} and H_{K_2}.
3. Gilbert's model holds true for each strip where internal coupling fields are included. The coupling fields arise when the normal component of the magnetization is not constant across an interface, i.e. $\nabla \cdot \bar{M} \neq 0$.

To calculate the interaction field it is further assumed that:

1. The strips are infinite in number and length.
2. The field calculated at the center of the strip is a good estimate of the interaction field.
3. The width of strips is >> the film thickness.

The surface magnetic charge density is equal to $M(\cos(\phi_1-s)-\cos(\phi_2-s))$ causing a field, $\bar{H}^1$, at b/2.

$$\bar{H}^1 = - \frac{tM}{\pi \mu_o b} (\cos(\phi_1-s)-\cos(\phi_2-s)) \bar{a}_s \qquad (51)$$

t --- film thickness

b ---strip width

$\bar{a}_s$---unit vector perpendicular to the interface

However, there are an infinite number of interfaces which contribute. Adding their respective fields,

$$\bar{H}_i^1 = \bar{H}_1 \left(1 + 1 - \frac{1}{3} - \frac{1}{3} + \frac{1}{5} + \frac{1}{5} \cdots\right) \tag{52}$$

$$\bar{H}_i^1 = -\frac{tM}{2b\ \mu_o} \left(\cos(\phi_1 - s) - \cos(\phi_2 - s)\right) \bar{a}_s \tag{53}$$

Similarly,

$$\bar{H}_i^2 = -\frac{tM}{2b\ \mu_o} \left(\cos(\phi_2 - s) - \cos(\phi_1 - s)\right) \bar{a}_s \tag{54}$$

Taking the ϕ component of these two fields and substituting them into Gilbert's equations 41 and 42, the final equations of motion for the strip domain model are

$$\frac{d\phi_1}{dt} = \frac{\alpha\gamma}{1+\alpha^2} H_\phi^1 + \frac{\gamma M}{(1+\alpha^2)\ \mu_o} \psi_1 \tag{55}$$

$$\frac{d\psi_1}{dt} = \frac{\gamma}{1+\alpha^2} H_\phi^1 - \frac{\alpha\gamma M}{(1+\alpha^2)\ \mu_o} \psi_1 \tag{56}$$

$$\frac{d\phi_2}{dt} = \frac{\alpha\gamma}{1+\alpha^2} H_\phi^2 + \frac{\gamma M}{(1+\alpha^2)\ \mu_o} \psi_2 \tag{57}$$

$$\frac{d\psi_2}{dt} = \frac{\gamma}{1+\alpha^2} H_\phi^2 - \frac{\alpha\gamma M}{(1+\alpha^2)\ \mu_o} \psi_2 \tag{58}$$

where

$$H_\phi^1 = -H_{applied} \sin(\phi_1 - \beta) - \frac{H_K^1}{2} \sin 2\phi_1 + \frac{Mt}{2b\ \mu_o} \left(\cos(\phi_1 - s) - \cos(\phi_2 - s)\right) \sin(\phi_1 - s) \tag{59}$$

H_ϕ^2 is obtained by interchanging number indices.

In essense, these are just the equations of motion for two films which are coupled magnetostatically.

Small angle calculation

The object here is to derive from a very simple model the effects of magnetization ripple on flux reversal. The model is grossly oversimplified, but does show clearly how a reaction torque arises from magnetostatic interactions.

Assume, Fig. 48,

1. A strip model where the strips are perpendicular to the initial magnetization.
2. The initial angles ϕ_1 and ϕ_2 are unequal due to random anisotropy variations other than H_K.
3. The angular difference between ϕ_1 and ϕ_2 to be constant during magnetization reversal. This exaggerates magnetostatic interaction, because the resulting high internal fields tend to allign the two magnetization vectors. However, the random anisotropies counteract this alligning influence so the assumption is plausible, at least for small ϕ_1 and ϕ_2.

To develop the equations of motion, the strip model equations of motion are rearranged, letting

$$\phi_1 = \langle\phi\rangle - \delta \qquad \delta \ll 1 \qquad (60)$$

$$\phi_2 = \langle\phi\rangle + \delta \qquad (61)$$

$$\psi_1 = \langle\psi\rangle - \varepsilon \qquad \varepsilon \ll 1 \qquad (62)$$

$$\psi_2 = \langle\psi\rangle + \varepsilon \qquad (63)$$

until the equations are interms of $\langle\phi\rangle$, $\langle\psi\rangle$, ε, and δ. In this process only first order terms in ε and δ will be retained.

Substituting 60, 61, 62, and 63 into equations 56 and 58 and then adding the results give

$$\frac{d}{dt}\langle\psi\rangle = \frac{\gamma}{1+\alpha^2}\left[-\frac{H_K}{2}\sin 2\langle\phi\rangle - H_{applied}\sin(\phi-\beta)\right.$$

$$\left. - \frac{Mt}{2b\,\mu_o}\sin^2\delta\,\sin 2(\phi-s)\right] - \frac{\alpha\gamma M}{(1+\alpha^2)\,\mu_o}\langle\psi\rangle \qquad (64)$$

Keeping only the dominate second term in equations 55 and 57 as was discussed for the Gilbert model, it immediately follows that

$$\frac{d}{dt}\langle\phi\rangle = \frac{\gamma M}{(1+\alpha^2)\,\mu_o}\langle\psi\rangle \qquad (65)$$

The only difference between equations 64, 65 and 41, 42 is the extra "reaction torque term" arising from the strip magnetostatic interactions. Also note the similarity in reaction torques between this calculation and Harte's equation 48.